



# Diet-driven microbial ecology underpins associations between cancer immunotherapy outcomes and the gut microbiome

Rebecca C. Simpson<sup>1,2,3,19</sup>, Erin R. Shanahan<sup>3,4,19</sup>, Marcel Batten<sup>1,2,5,19</sup>, Irene L. M. Reijers<sup>6</sup>, Mark Read<sup>1,3,7,8</sup>, Ines P. Silva<sup>1,9</sup>, Judith M. Versluis<sup>6</sup>, Rosilene Ribeiro<sup>3,4</sup>, Alexandra S. Angelatos<sup>3,10</sup>, Jian Tan<sup>3,10</sup>, Chandra Adhikari<sup>1</sup>, Alexander M. Menzies<sup>1,2,11</sup>, Robyn P. M. Saw<sup>1,2,12</sup>, Maria Gonzalez<sup>1</sup>, Kerwin F. Shannon<sup>1,12</sup>, Andrew J. Spillane<sup>1,4,13</sup>, Rebecca Velickovic<sup>1,2</sup>, Alexander J. Lazar<sup>1,14,15</sup>, Ashish V. Damania<sup>15</sup>, Aditya K. Mishra<sup>15</sup>, Manoj Chelvanambi<sup>16</sup>, Anik Banerjee<sup>17</sup>, Nadim J. Ajami<sup>15</sup>, Jennifer A. Wargo<sup>15,16</sup>, Laurence Macia<sup>1,3,10</sup>, Andrew J. Holmes<sup>3,4</sup>, James S. Wilmott<sup>1,2,3</sup>, Christian U. Blank<sup>6</sup>, Richard A. Scolyer<sup>1,2,3,18</sup> and Georgina V. Long<sup>1,2,3,11</sup>✉

**The gut microbiota shapes the response to immune checkpoint inhibitors (ICIs) in cancer, however dietary and geographic influences have not been well-studied in prospective trials. To address this, we prospectively profiled baseline gut (fecal) microbiota signatures and dietary patterns of 103 trial patients from Australia and the Netherlands treated with neoadjuvant ICIs for high risk resectable metastatic melanoma and performed an integrated analysis with data from 115 patients with melanoma treated with ICIs in the United States. We observed geographically distinct microbial signatures of response and immune-related adverse events (irAEs). Overall, response rates were higher in *Ruminococcaceae*-dominated microbiomes than in *Bacteroidaceae*-dominated microbiomes. Poor response was associated with lower fiber and omega 3 fatty acid consumption and elevated levels of C-reactive protein in the peripheral circulation at baseline. Together, these data provide insight into the relevance of native gut microbiota signatures, dietary intake and systemic inflammation in shaping the response to and toxicity from ICIs, prompting the need for further studies in this area.**

Combination ICIs that block PD-1 and CTLA-4 are highly effective against metastatic melanoma and many other advanced cancers<sup>1</sup>, leading to more-effective responses compared to either treatment alone<sup>2–6</sup>. Recently, this combination has also shown promise as a neoadjuvant treatment for stage III melanoma, with high pathological response rates and a low rate of recurrence<sup>7–9</sup>. At present, the broad application of this dual therapeutic approach for many patients is limited by the high rate of irAEs<sup>3–5,10</sup>. The ability to predict responses to immunotherapy and to prevent the development of severe toxicities would allow this therapy to be implemented in a larger, diverse cohort of patients and at earlier stages of disease and would reduce life-altering morbidities due to toxicity. The intestinal microbiota has a systemic role in immune regulation<sup>11–16</sup> and is known to influence the development of a variety of inflammatory disorders<sup>17</sup>.

Although there is growing evidence highlighting a role for the gut microbiome during immunotherapy, previous studies have lacked agreement as to the key microbial drivers of response and resistance<sup>18–25</sup>. Various statistical approaches have been utilized to highlight the discord between geographically distinct cohorts<sup>26,27</sup>. However, the biology underpinning this discordance remains unclear. Common microbial ecosystem features linking responses across studies are yet to be identified<sup>28</sup>, and the delineation of irAE-protective microbial patterns are lacking, particularly in the neoadjuvant setting. Here, we study the associations between the gut microbiota and immunotherapy response and irAE development using a clinically homogenous trial cohort of patients in Australia and the Netherlands who presented with melanoma treated with neoadjuvant combination ICIs. We also validate the intercontinental discordance in the data from patients in

<sup>1</sup>Melanoma Institute Australia, The University of Sydney, Sydney, Australia. <sup>2</sup>Sydney Medical School, Faculty of Medicine and Health, The University of Sydney, Sydney, Australia. <sup>3</sup>Charles Perkins Centre, The University of Sydney, Sydney, Australia. <sup>4</sup>School of Life and Environmental Science, Faculty of Science, The University of Sydney, Sydney, Australia. <sup>5</sup>Faculty of Medicine and Health, The University of Sydney, Sydney, Australia. <sup>6</sup>Department of Medical Oncology, Netherlands Cancer Institute, Amsterdam, The Netherlands. <sup>7</sup>School of Computer Science, The University of Sydney, Sydney, Australia. <sup>8</sup>The Westmead Initiative, The University of Sydney, Sydney, Australia. <sup>9</sup>Westmead and Blacktown Hospitals, Sydney, Australia. <sup>10</sup>School of Medical Sciences, Faculty of Medicine and Health, The University of Sydney, Sydney, Australia. <sup>11</sup>Department of Medical Oncology, Royal North Shore and Mater Hospitals, Sydney, Australia. <sup>12</sup>Department of Melanoma and Surgical Oncology, Royal Prince Alfred Hospital, Sydney, Australia. <sup>13</sup>Breast and Melanoma Surgery Department, Royal North Shore Hospital, St Leonards, Australia. <sup>14</sup>Department of Pathology and Laboratory Medicine, The University of Texas MD Anderson Cancer Center, Houston, TX, USA. <sup>15</sup>Platform for Innovative Microbiome and Translational Research, Department of Genomic Medicine, The University of Texas MD Anderson Cancer Center, Houston, TX, USA. <sup>16</sup>Department of Surgical Oncology, The University of Texas MD Anderson Cancer Center, Houston, TX, USA. <sup>17</sup>The University of Texas MD Anderson UTHealth Graduate School of Biomedical Sciences, Houston, TX, USA. <sup>18</sup>Tissue Pathology and Diagnostic Oncology, Royal Prince Alfred Hospital and NSW Health Pathology, Sydney, Australia. <sup>19</sup>These authors contributed equally: Rebecca C. Simpson, Erin R. Shanahan, Marcel Batten. ✉e-mail: [georgina.long@sydney.edu.au](mailto:georgina.long@sydney.edu.au)

Australia and the Netherlands with previously published datasets from patients in the United States.

## Results

**Patients and treatment.** To assess the relationship between microbiome metrics and patient outcomes after combination PD-1 and CTLA-4 blockade, we first characterized pre-treatment fecal microbiomes collected as a part of a prospective clinical trial from 71 Australian and 32 Dutch patients with melanoma receiving neoadjuvant ipilimumab and nivolumab in a clinical trial (OpACIN-neo and PRADO extension cohort, NCT02977052)<sup>7</sup>. All data were collected prospectively, including stool samples, dietary surveys, tumor response and ICI-associated toxicity. Given the strict trial eligibility, the patient characteristics were highly homogeneous; all had RECIST-measurable stage III cutaneous melanoma, with local lymph node involvement only, no in-transit disease, no previous immunotherapy, normal lactate dehydrogenase (LDH) and Eastern Cooperative Oncology Group (ECOG) 0–1 (Supplementary Table 1). All patients were treated with nivolumab (anti-PD-1) combined with ipilimumab (anti-CTLA-4) (as per dosing strategies in Supplementary Tables 1 and 2). Fecal samples were collected prior to treatment and affected lymph nodes were resected (either complete lymph node dissection or index lymph node resection) at the end of the 6-week treatment program (Methods and Extended Data Fig. 1). Patients were characterized to enable categorization into three clinically relevant dichotomies: responders (R) (complete, near-complete or partial pathological response) or non-responders (NR) (pathological non-response) based on the pathological assessment of resection specimens after neoadjuvant therapy (Supplementary Table 3)<sup>29,30</sup>; mild (grade 0–2) or severe irAEs (had at least one serious irAE grade  $\geq 3$ ) (Supplementary Tables 2 and 3)<sup>7</sup>; and beneficial or benign (all R or NR with mild irAEs) or adverse (NR with severe irAEs). This latter group is important since irAEs can also indirectly impact the efficacy of treatment by leading to discontinuation of therapy and administration of immunosuppressive drugs. The identification of such patients prior to treatment is therefore highly clinically relevant and represents an urgent unmet clinical need, so that unnecessary toxicity and a futile therapy may be avoided, and therapies with a higher chance of success are not delayed.

**Gut microbiome associations with response and toxicity.** This study examines associations between the gut microbiome with ICI treatment outcomes in a homogenous trial population across two continents. This is particularly relevant given the apparent lack of consensus across previous studies, in which both clinical heterogeneity and geography may confound outcome associations with the microbiome. Notably, when clinical factors that could potentially confound the relationship between outcome response and the gut microbiome were assessed in the present study, no significant association was identified (Supplementary Table 4). Furthermore, these parameters were also not significantly different between the Australian and Dutch patients (Supplementary Table 5). To further study geographical effects, analysis was expanded to a third continent using published United States cohorts of patients with metastatic melanoma treated with ICIs ( $n=115$ ) (Fig. 1a). We first performed 16S-amplicon-based community profiling of all Australian patient baseline fecal microbiomes ( $n=71$ ) (Extended Data Fig. 2a,b). In a previous study of anti-PD-1-treated stage IV patients with melanoma, low microbiome diversity was linked to non-response<sup>19</sup>. No significant differences were identified in alpha-diversity metrics between R and NR groups (Fig. 1b) or between mild, severe, benign and adverse irAE groups (Extended Data Fig. 2c). However, patients that were NR that developed severe irAEs (adverse) had significantly lower microbiome diversity at baseline ( $P=0.0157$ ) (Fig. 1c and Extended Data Fig. 2d). Data from patients who developed

severe gastrointestinal (GI) irAEs (colitis and gastritis) contributed most to this effect ( $P=0.0605$ ) (Extended Data Fig. 2e). When stratifying patients using tumor mutational burden (TMB) as a tumor-intrinsic biomarker associated with response, we found that NR with high TMB had significantly lower diversity than R with high TMB ( $P=0.0049$ ) (Extended Data Fig. 2f-h), suggesting the potential importance of tumor-extrinsic mechanisms, such as the gut microbiome, in determining response to immunotherapy.

We next assessed the association between total bacterial load and clinical outcomes using quantitative PCR (qPCR) targeting the 16S rRNA gene. We observed a reduction in total bacterial load per mg of feces in NR ( $P=0.0170$ ) (Fig. 1d and Extended Data Fig. 2i-k). Compositional differences between the three clinical dichotomies (response, irAE grade, and combined response and toxicity) were assessed using linear discriminant analysis effect size (LEfSe) and validated using taxa-specific qPCR (Extended Data Fig. 3a-h). Taxa that were significantly enriched in the gut microbiome of R included *Faecalibacterium prausnitzii*, *Butyrivibrio pullicaerorum* and *Akkermansia muciniphilia* ( $P=0.0066$ ,  $P=0.0049$  and  $P=0.0309$ , respectively, Fig. 1e-g), which overlap with those that have been identified in previous immunotherapy studies<sup>19,20,22,24,31,32</sup>. Our data indicate that there is an overlap between microbes linked with response and microbes linked with protection from developing irAEs. For example, *F. prausnitzii* abundance was also reduced in patients that developed severe irAEs ( $P=0.0526$ ), particularly in those patients that were both NR and that developed severe irAEs (adverse) ( $P=0.0200$ ) (Extended Data Fig. 3g). Patients in the adverse outcome group had a reduced relative abundance of taxa in the *Clostridiales* order (Extended Data Fig. 3e,f). This pattern was largely due to the reduced relative abundance of amplicon sequence variants (ASVs) classified to taxa within the *Ruminococcaceae* (*Faecalibacterium prausnitzii*, *Oscillospira* and *Ruminococcus bromii*) and *Lachnospiraceae* families. A similar association with reduction in these microbial features has also been reported for inflammatory bowel disease<sup>33,34</sup>.

The 16S amplicon sequencing also identified two archaeal ASVs, both *Methanobacteriaceae*, that appeared to be differentially represented within the Australian cohort. This was explored further using qPCR, and we found that patients tended to fall into high-methanogen-abundance or low-methanogen-abundance groups. Notably, all patients in the adverse outcome group had low methanogen abundance, and, overall, methanogens were significantly reduced in patients who developed severe irAEs (Extended Data Fig. 4a-d). A keystone community process for optimal bacterial fermentative metabolism [for example- breakdown of dietary carbohydrates by members of the *Ruminococcaceae* family] is removal of the byproduct hydrogen. Methanogens are important contributors to this process, facilitating the maintenance of a diverse intestinal tract ecosystem<sup>35,36</sup>. We found that all patients in the adverse group had both low diversity and low abundance of methanogens, and both metrics were also overrepresented in the severe irAEs group. We postulate that this pattern might reflect fundamental differences in community level metabolic output in the presence or absence of methanogens that influence the host-microbiome relationship in the context of immunotherapy.

**Nutritional input and microbial metabolism.** Given that diet is a key factor that shapes the composition and function of the microbiome<sup>37,38</sup>, food frequency questionnaires were prospectively collected and used to estimate nutritional input. Nutritional data were collected from 60 of the 71 Australian patients. Key macronutrients and micronutrients were assessed in accordance with Australian dietary recommendations. Analysis indicated that most patients, irrespective of response, consumed suboptimal diets that do not meet the nutritional guidelines, as evidenced by low fiber consumption and high sugar and saturated fat consumption (Extended Data

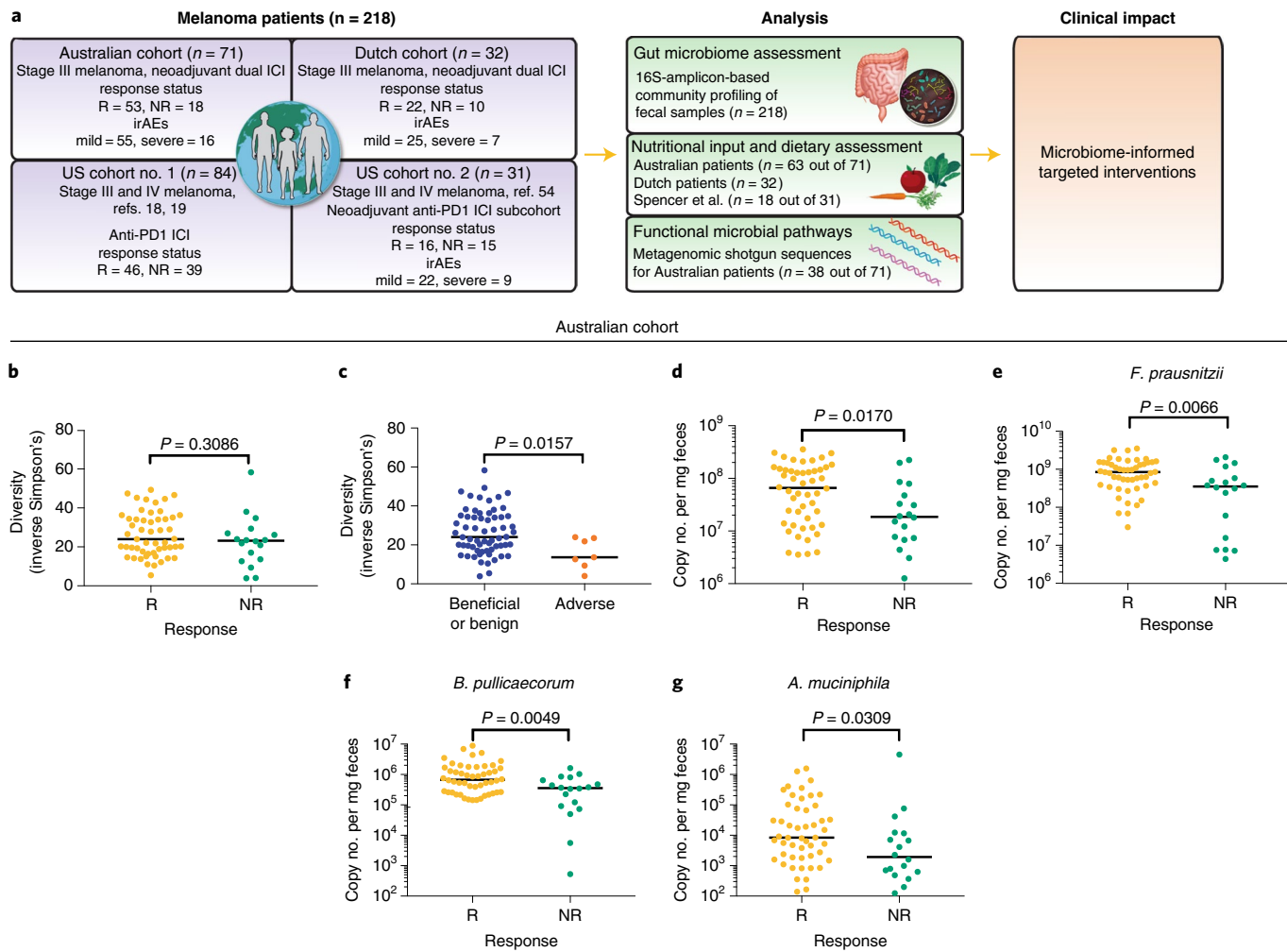


**Fig. 1 | Associations between gut microbiota and treatment response and irAEs in Australian patients with melanoma.** **a**, Schematic overview of the study<sup>54</sup>. **b,c**, Bacterial community profiling of patient baseline fecal samples via 16S rRNA gene amplicon sequencing (AUS, n = 71). Inverse Simpson's index of alpha-diversity for individual patients grouped by R and NR (**b**) and beneficial or benign (all R or NR irAEs < G3) and adverse (NR, irAEs ≥ G3) outcomes (**c**). **d**, Absolute bacterial fecal loads assessed using qPCR were used to determine bacterial copy number per mg feces and were grouped according to response (n = 71). **e–g**, qPCR using taxa-specific primers was used to determine bacterial copy number per mg feces of selected taxa identified using LEfSe analysis grouped according to response (n = 71). Each symbol represents data from an individual patient; bars indicate the median. For **b–g**, Mann-Whitney U rank sum test was used. All statistical tests are two-sided where appropriate.

Fig. 5a–i). Notably, significantly lower omega 3 consumption was observed in both NR (Fisher's exact test,  $P=0.0139$ ) (Fig. 2a,b) and adverse outcome groups (Fisher's exact test,  $P=0.0259$ )<sup>39</sup> (Fig. 2b,c). Indeed, microbial diversity correlated with omega 3 consumption ( $P=0.0429$ ) (Fig. 2e) to a greater extent than fiber consumption ( $P=0.0764$ ) (Fig. 2f). Fiber consumption positively correlated with the abundance of *Ruminococcaceae* ( $P=0.0309$ ) (Fig. 2g). Fiber and omega 3 are both dietary components that have previously been linked to promoting intestinal integrity, enhancing short chain fatty acid (SCFA) production and altering the inflammatory state of the gut<sup>14,38,40–43</sup>. While causality of the fiber and omega 3 effects will require dedicated prospective trials, our data suggest that these nutrients are associated with a diverse microbiome that exhibits the hallmarks of health and intestinal homeostasis, and that is associated with a response in the absence of severe toxicities.

Given that differences in microbiome composition and diet are suggestive of altered microbial ecosystem function, we investigated the metabolic potential of patient microbiomes. We performed metagenomic shotgun sequencing on a subset of 38 fecal DNA samples from Australian patients (OpACIN-neo trial,

with metabolic pathways defined based on the MetaCyc hierarchy of pathways. Microbial functional pathways that were significantly differentially represented between beneficial or benign and adverse outcome groups were identified (Extended Data Fig. 6a,b). Pathways that were reduced in the *adverse* outcome group included those pertaining to SCFA butyrate (butanoate) production, B vitamin synthesis, purine degradation and amino acid synthesis (Fig. 2h–k). Notably, changes to purine metabolism and recycling have recently been suggested to be important for the efficacy of immunotherapy<sup>44</sup>, and B vitamin synthesis has been associated with protection from colitis<sup>45</sup>. Pathways were also identified as overrepresented within the *adverse* outcome group (Extended Data Fig. 6a); however, upon inspection in individual patients, the relative abundance of genes in these pathways were highly heterogeneous (Extended Data Fig. 6b). These data support the hypothesis that the risk of *adverse* outcome is associated with reduced representation of beneficial metabolic capabilities of the microbiome. Butyrate is a primary colonocyte energy source that is important for maintaining epithelial integrity and intestinal homeostasis<sup>14,46</sup>. Three specific butyrate production pathways

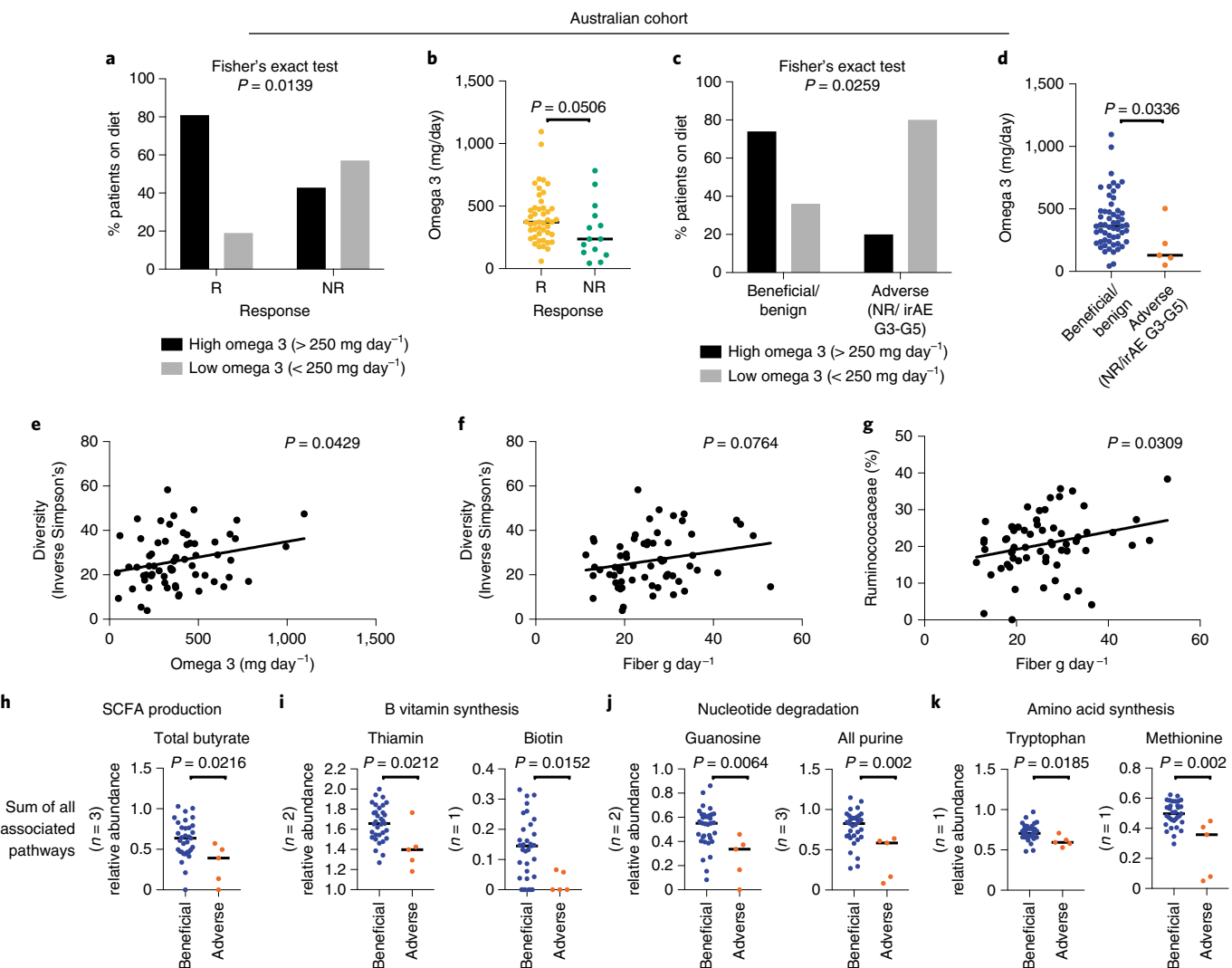


**Fig. 2 | Microbial functions and dietary nutrient intake that promote gut integrity are associated with protection from irAEs and lack of response.**

**a-d**, Omega 3 consumption ( $\text{mg day}^{-1}$ ) was estimated from food intake surveys (AUS,  $n=63$ ). Patients were categorized according to low or high omega 3 dietary intake, according to the Australian dietary recommendations and were grouped according to response (a) or beneficial or benign or adverse outcome groupings (c). Fisher's exact test (conducted on total number of patients per group). For b and d, raw estimated omega 3 consumption ( $\text{mg day}^{-1}$ ) grouped by R (yellow) or NR (green) (b), and beneficial or benign (blue) or adverse (orange) outcomes (d). e-f, Correlations of omega 3 and fiber consumption and diversity. g, Correlation of fiber consumption against the relative abundance of *Ruminococcaceae*. h-k, MetaCyc pathways were predicted in the metagenomes of fecal samples of a subset of 38 Australian patients. LDA scores for differentially abundant pathways in the beneficial or benign (all R or NR irAEs < G3) and adverse (NR, irAEs  $\geq$  G3) outcome groups were determined by LEfSe analysis. The relative abundance of pathways identified as significant that result in a common metabolic output were added together and shown for individual patients ( $n=38$ ). Each symbol represents an individual patient, bars indicate the median. P values indicated. For b, d and g-k, Mann-Whitney U rank sum test was used. For linear regressions, P value was calculated using Spearman's rank correlation (e-g). All statistical tests are two-sided where appropriate.

were significantly associated with beneficial or benign outcomes (Extended Data Fig. 6a). Combining these into a single metabolic indicator revealed that the prevalence of butyrogenesis was significantly reduced in *adverse* outcome patients (Fig. 2h). This aligns with the observed reduction in known key butyrate-producing *Ruminococcaceae* and *Lachnospiraceae* family taxa (Extended Data Fig. 3e,f). Fecal butyrate levels determined using nuclear magnetic resonance spectroscopy (NMR) correlated with the relative abundance of CENTFERM butyrate synthesis pathway genes (Extended Data Fig. 7a). Serum butyrate levels, however, were not significantly different between adverse and beneficial or benign groups, or in NR overall (Extended Data Fig. 7b,c). Serum butyrate levels are impacted by both microbial production in the gut and consumption by colonocytes, and excess SCFA in the

systemic circulation (in contrast to the gut) may be linked to sub-optimal immunotherapy responses, as observed in a recent study<sup>23</sup>.

**Effects of geography on the microbiome.** To validate which microbiome outcome associations might be generalized to independent cohorts, microbial signatures associated with response and irAE development in the Australian cohort were assessed in a cohort of Dutch patients with melanoma ( $n=32$ ) participating in the same prospective international neoadjuvant clinical trial (PRADO, NCT02977052). No significant differences in diversity between outcome groups were identified (Fig. 3a). Furthermore, *F. prausnitzii*, *B. pullucacorum* and *A. muciniphilia* were not present in reduced abundance in Dutch NR (Fig. 3b). A similar difference in the taxa associated with response and irAEs was identified when LEfSe was

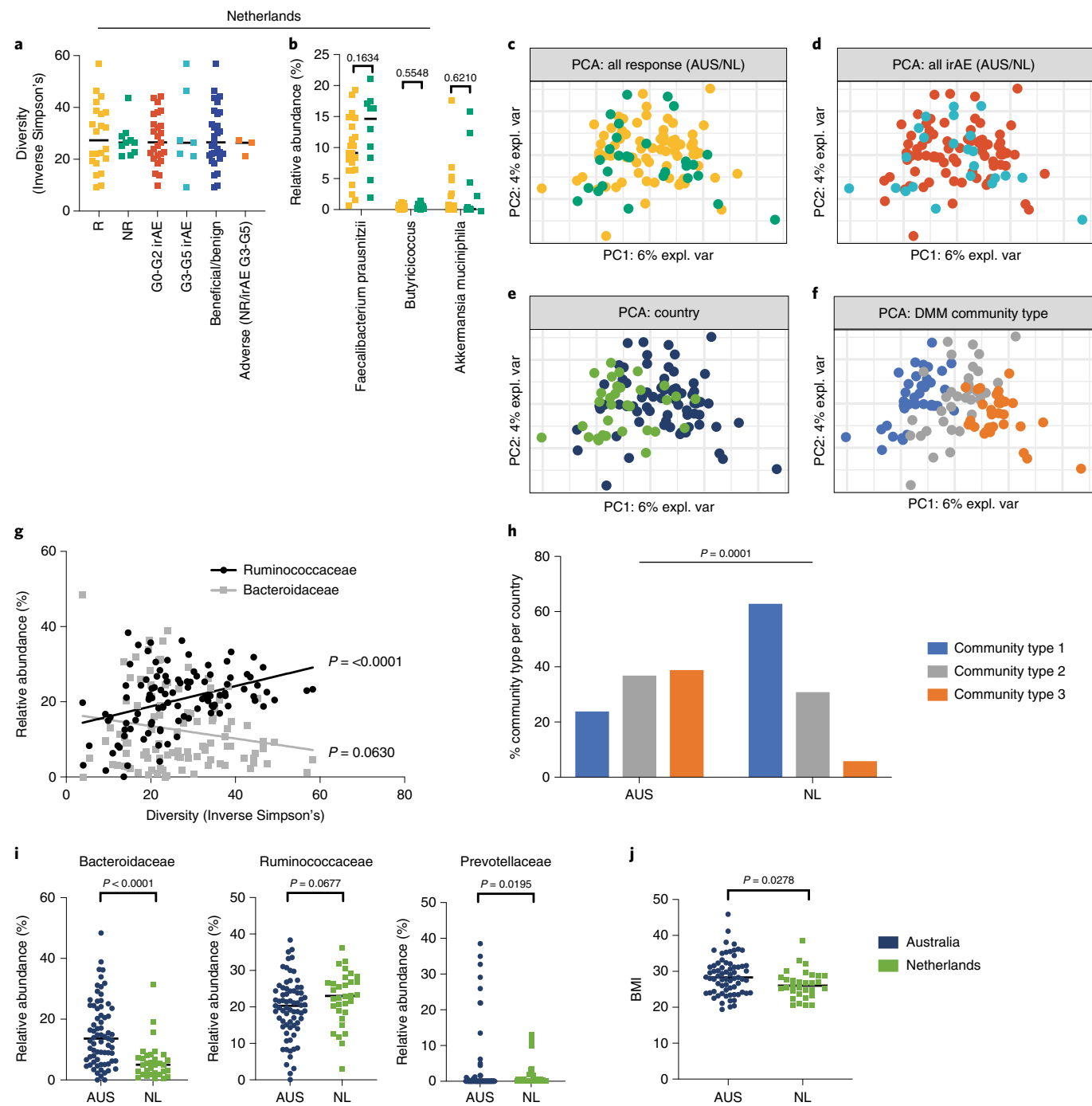


**Fig. 3 | Geographical differences in microbial communities in cohorts from Australia and the Netherlands.** **a**, Inverse Simpson's diversity scores for Dutch patients ( $n=32$ ) stratified by response, irAEs and beneficial or benign or adverse outcome groupings. **b**, Relative abundance of key taxa associated with treatment response from the Australian cohort assessed in the Dutch cohort ( $n=32$ ). **c–e**, Beta-diversity of microbiomes from the combined cohort (Australian and Dutch,  $n=103$ ) shown through PCA plots colored by treatment response (**c**), irAEs (**d**) and country (**e**). Colors correspond to the legend as indicated. **f**, DMM was used to stratify patient microbiomes ( $n=103$ ) and assess the optimal number of clusters present in the provided dataset. PCA plot of patient's microbiomes, colored according to DMM community type; community type 1 (blue), community type 2 (grey) and community type 3 (orange). **g**, Relative abundance of Bacteroidaceae or Ruminococcaceae correlated with inverse Simpson's diversity.  $P$  value was calculated using Spearman's rank correlation. **h**, Percentage distribution of community types per country. Fisher's exact test (conducted on the total number of patients per group). **i**, Relative abundance of Bacteroidaceae, Ruminococcaceae and Prevotellaceae by country (Australian,  $n=71$ , NL  $n=32$ ). **j**, Patient BMI by country (Australian,  $n=71$ , NL  $n=32$ ). Each symbol represents an individual patient; bars indicate the median. For **a–b** and **i–j**, Mann-Whitney U rank sum test. FDR-adjusted  $P$  values indicated. All statistical tests are two-sided where appropriate. AUS, Australian; NL, Dutch.

used to identify compositional differences between clinical outcome groupings (Extended Data Fig. 7d–g and Supplementary Table 6). For example, some taxa classified within the *Ruminococcaceae* genera

that were observed in R and associated with protection from adverse outcomes in Australian patients (Extended Data Fig. 3) were enriched in Dutch patients who developed severe toxicities

(Extended Data Fig. 7f,g). This issue of geography-dependent outcome associations has been reported in previous studies<sup>27,47</sup>. Such heterogeneity severely limits the utility of microbiome signatures in the clinic and intervention management.

Increasing evidence supports the concept that intrinsic properties of an individual's microbiome constrains relationships with host traits (for example, immune tone) and selective pressure, such as diet<sup>48</sup>. We therefore explored whether differences in microbial community assembly could explain the observed differences in microbial associations with clinical outcomes between patients from Australia and the Netherlands. Across the combined cohort ( $n=103$ ), we found no significant clustering of microbiomes by treatment response or irAE status at the whole-community level (Fig. 3c,d). There was also no significant separation between the Australian and Dutch patient microbiomes at a whole-community level (Fig. 3e and Extended Data Fig. 8a). Therefore, to stratify patient microbiomes ( $n=103$ ), the dirichlet multinomial mixtures (DMM)<sup>49</sup> was used to assess the optimal number of clusters present in the overall dataset. This method identified three microbial 'community types' which formed significant clusters in ordination space, independent of geographical origin (Fig. 3f and Extended Data Fig. 8a,b). This indicates that intrinsic assembly pattern, rather than country of habitat, is a stronger determinant of microbial community structure. Of the three gut microbial 'community types' identified, community type 1 is characterized by high alpha-diversity and a high ratio of *Ruminococcaceae* to *Bacteroidaceae*, whereas community type 3 is characterized by low diversity and a low ratio of *Ruminococcaceae* to *Bacteroidaceae* (Extended Data Fig. 8c–l). Further supporting this, the relative abundance of *Ruminococcaceae* positively correlated with diversity, whereas *Bacteroidaceae* negatively correlated with diversity ( $P<0.0001$ ,  $P=0.0630$ ) (Fig. 3g and Extended Data Fig. 9a–c). Notably, there was a marked difference in the distribution of these community types between the countries ( $\chi^2 P=0.0001$ ) (Fig. 3h). Gut microbiomes of Dutch patients were predominantly community type 1, whereas those of Australian patients were more evenly distributed. This highlights the fundamental difference in distribution of microbial community compositions between the Australian and Dutch patients. Given the links between long-term diet and microbial ecosystem structure<sup>50,51</sup>, dietary intake probably contributes to this effect, with evidence of higher fiber consumption being associated with community type 1 ( $P=0.0044$ ) compared to community type 3 ( $P=0.0519$ ) in both countries (Extended Data Fig. 9d,e). Furthermore, Australian patients had significantly higher relative abundances of *Bacteroidaceae* compared to Dutch patients ( $P<0.0001$ ) (Fig. 3i), which has previously been associated with a more 'Western-style' diet (high animal fat and protein and low fiber)<sup>52</sup>. Indeed, Dutch patients had significantly lower BMIs than Australian patients ( $P=0.0278$ ) (Fig. 3j).

These observations suggest that variance in the assemblage of microbial communities confounds the identification of generalizable associations between the gut microbiome and treatment

response and irAE development. To further assess this, we employed machine learning to generate microbial signatures of response and severe irAE development, derived from baseline 16S rRNA gene profiles. In the total cohort ( $n=103$ ), these could correctly identify outcomes with a mean prediction accuracy of 61.2% (response) and 63.6% (irAEs), respectively (Extended Data Fig. 9f,g). Notably, however, stratifying patients into latent classes based on community types, but not countries, prior to conducting machine learning increased the prediction accuracy and robustness of the models assessed via randomization testing (leave-one-out cross validation) in most cases (Extended Data Fig. 9f,g). This is despite these models being based on only approximately one-third of the patient cohort in each case, which normally would be expected to significantly reduce model performance<sup>53</sup>. In addition, the microbial signatures indicative of response and irAE development within each 'community type' were unique (Supplementary Tables 7–12), suggesting an ecological context dependency.

**Diet-driven microbial ecology and immunotherapy response.** Given that *Ruminococcaceae* and *Bacteroidaceae* families were the key taxa driving the DMM clusters, we stratified individuals according to the comparative relative abundance of these two taxa. Consistent with this, microbiomes with a higher relative abundance of *Ruminococcaceae* also had significantly higher diversity ( $P<0.0001$ ) and methanogen abundance ( $P=0.0029$ ) and were associated with significantly higher fiber consumption ( $P=0.0331$ ) (Fig. 4a,b). Enhanced relative abundance of mucin degradation genes was observed in patients with *Bacteroidaceae*-dominated-microbiomes ( $P=0.0001$ ) (Fig. 4a). Furthermore, we also observed that *Bacteroidaceae*-dominated-microbiomes were associated with significantly higher levels of C-reactive protein (CRP) in patients at baseline ( $P=0.0180$ ) (Fig. 4c), suggesting a link between microbial community ecology and local and systemic inflammatory tone prior to ICI treatment.

This simplified and robust stratification approach allows further comparison of our cohort to previously published 16S datasets. Analysis of data from patients with metastatic melanoma in the United States treated in both neoadjuvant and non-neoadjuvant settings ( $n=31$ , ref. <sup>54</sup>;  $n=84$ , ref. <sup>19</sup> and ref. <sup>18,19,54</sup>) confirmed that marked differences in community structure occur in cohorts from Australia, the Netherlands and the United States ( $\chi^2 P<0.0001$ ) (Fig. 4d). Of note is the near absence of high-diversity *Ruminococcaceae*-dominated gut microbiomes in the United States cohort and the near absence of low-diversity *Bacteroidaceae* gut microbiomes in the Dutch cohort (Extended data Fig. 10a–d). Given these observations, we next assessed whether differences in overall microbial community structure correlate with clinical outcomes. Higher rates of response to ICI therapy were associated with *Ruminococcaceae*-dominated gut microbiomes compared to *Bacteroidaceae*-dominated gut microbiomes across the combined Australian, Dutch and United States

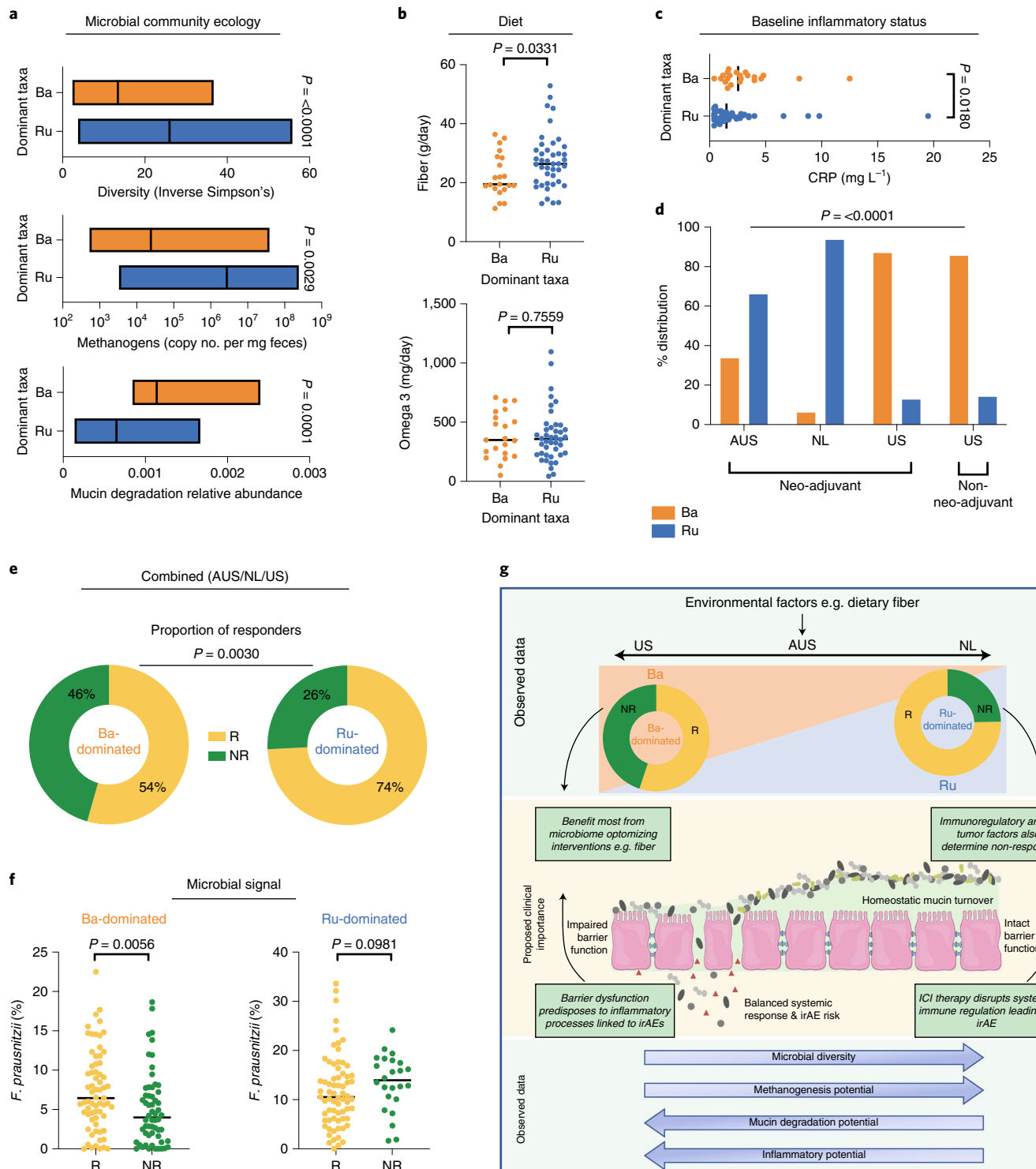
**Fig. 4 | Ruminococcaceae-associated microbial signatures support the response to checkpoint inhibitor immunotherapy.** Individuals were stratified according to the comparative relative abundance of *Bacteroidaceae* (Ba) and *Ruminococcaceae* (Ru). **a**, Differences in community ecology between microbiomes dominated by Ba or Ru. Inverse Simpson's diversity (top), methanogen load expressed as copy number per mg feces (middle) (Australian and Dutch,  $n=103$ ), and relative abundance of mucin degradation pathways identified in metagenomics sequencing (Australian,  $n=38$ ) (bottom). Box plots are shown as a median bar and box indicating minimum and maximum values. **b**, Estimated fiber (g day<sup>-1</sup>) (top) and omega 3 (mg day<sup>-1</sup>) consumption from food intake surveys (Australian,  $n=63$ ) grouped by dominant taxa grouping. **c**, Baseline CRP by dominant taxa grouping (Ba or Ru) (Australian,  $n=71$ ). **d**, Distribution of Ba and Ru dominated microbiomes by country ( $n=218$ ). Data from the United States containing previously published 16S amplicon datasets of metastatic melanoma ( $n=31$  neoadjuvant cohort (ref. <sup>54</sup>) and  $n=84$  non-neoadjuvant (ref. <sup>19</sup> and ref. <sup>18</sup>)). Chi-squared test (conducted on total number of patients per group). **e**, Distribution of response or non-response within dominant taxa groupings (Ba and Ru) (Australian, Dutch, and US,  $n=218$ ). Fisher's exact test (conducted on total number of patients per group). **f**, Relative abundance of *F. prausnitzii* for individual patients by response (R versus NR) within dominant taxa groups (Ba and Ru) (Australian, Dutch, and US,  $n=218$ ). Each symbol represents data from an individual patient; bars indicate the median. For **a–c** and **f**, Mann-Whitney U rank sum test was used. All statistical tests are two-sided where appropriate. **g**, Summary and proposed model of diet-microbiome-host interactions during immunotherapy. AUS, Australian; NL, Dutch.

cohorts (Fisher's exact test,  $P=0.0030$ ) (Fig. 4e). Interestingly, stratifying the patients in this way also indicated that a significant reduction in the relative abundance of *Faecalibacterium prausnitzii* ( $P=0.0056$ ) and *Ruminococcaceae* ( $P=0.0006$ ) occurred in NR, but only within *Bacteroidaceae*-dominated gut microbiomes. In contrast, higher levels of *F. prausnitzii* did not offer further benefit in *Ruminococcaceae*-dominated microbiomes (Fig. 4f, Extended data Fig. 10e,f). These differential associations were also observed for the group of patients with adverse outcomes (Extended data Fig. 10h,i). Together, these data highlight that the overall assembly of microbial

communities, influenced by diverse environmental inputs such as diet, is an important factor in ICI therapy outcome (Fig. 4g) and may help to explain the differences in taxa associations observed across various cohorts<sup>18–20</sup>.

## Discussion

We have used a highly homogeneous prospective clinical trial cohort to show that a gut microbiome associated with higher fiber and omega 3 consumption is beneficial to facilitating optimal anti-tumor immune responses and minimizing the risk of irAEs



during immunotherapy. Microbial diversity and relative abundances of *Ruminococcaceae* family taxa, *Akkermansia muciniphila* and methanogenic archaea were significantly reduced in NR as well as in patients that developed severe toxicities. These features represent markers of robust symbiosis enriched with beneficial microbial functions and have been linked with homeostatic mucin turnover and the maintenance of epithelial integrity<sup>14</sup>, which are critical for the regulation of immune processes both locally and systemically.

Furthermore, by exploring the biology underpinning the microbiomes of patients across three continents, we demonstrate that variance in microbial signatures of immunotherapy response and irAE development between countries could be explained by the underlying differences in gut microbial community ecology, independent of geography. Notably, higher response rates were associated with *Ruminococcaceae*-dominated microbiomes, which had significantly higher microbial alpha-diversity and correlated with higher fiber consumption, reduced abundance of mucin degradation genes and lower levels of baseline CRP. This highlights the influence of diet and underlying microbial community structure on the relationship between gut microbes, the generation of optimal anti-tumor immune responses and the risk of irAEs during immunotherapy. Consistent with this, higher dietary fiber was associated with significantly improved progression-free survival in a cohort of ICI-treated patients from the United States<sup>54</sup>. Recurrent links have been observed between *Ruminococcaceae* family taxa or microbial community structures with higher relative abundance of *Oscillospiraceae* and *Ruminococcaceae*, and improved immunotherapy response<sup>25,26,54</sup>. In addition, a recent study suggested that microbiomes enriched with lipopolysaccharide synthesis and mucus degradation genes were associated with higher levels of systemic inflammation (neutrophil to lymphocyte ratio) and a poor response to anti-PD-1 immunotherapy<sup>26</sup>. Together, this suggests that the gut microbiome plays a role in establishing local and systemic immune tone prior to and during immunotherapy.

These findings are highly relevant because individual responses to a particular dietary intervention have been shown to be dependent on the baseline microbiome<sup>55,56</sup>. Additionally, the ability of probiotic strains or fecal microbiota transplants (FMTs) to successfully engraft is strongly influenced by the native microbiome<sup>57</sup>. Accounting for differences in the assemblage of microbial communities will therefore be important to reproducibly target the microbiome in the clinic to improve immunotherapy outcomes. We present a framework to overcome interindividual variation by accounting for ecological context, which could allow for the design of interventions to improve clinical outcomes that are more targeted. We hypothesize that increasing the dietary fiber intake of patients will have greater clinical benefit for those with *Bacteroidaceae*-dominated microbiomes, such as individuals from Australia and the United States, than for those who already have fiber-imprinted microbiomes, such as individuals from the Netherlands. Promisingly, a recent preclinical study showed that modulating the microbiome with a high-fiber diet could trigger innate cell reprogramming in the tumor microenvironment and induce type I interferon production, promoting the efficacy of immunotherapy<sup>58</sup>.

Attempts to identify specific microbial taxonomic biomarkers and develop predictive models based on microbiome data are frequently underpinned by the assumption that all microbiomes belong to a single class that respond according to the same ‘rules’. This is poorly justified and has frustrated efforts to use microbial data in the clinical setting<sup>55,56</sup>. Previous studies of microbial associations with response to immunotherapy in metastatic patients with melanoma have lacked consensus<sup>18–20,22,31</sup>. These studies were also highly clinically heterogeneous in terms of disease stage, line of therapy and the type of immunotherapy received, which may have confounded the findings regarding the microbiome. Notably, recent studies have further illustrated that no single microbial taxon alone

could be regarded as a fully predictive biomarker across cohorts<sup>26,27</sup>, even within a single country (United States), but instead that distinct community clusters may be favorable or unfavorable<sup>26</sup>. This supports our theory that microbial community ecology affects both treatment outcomes and the role and predictive power of various microbes. Together, these findings prompt further investigation, in the immunotherapy setting, of the relationship between microbial community structures, their impact on local and systemic immune responses and the ability to integrate stratification of patient microbiomes reproducibly in the clinic.

Although there is growing evidence, including the findings in the present work, that supports a role for the gut microbiome in determining outcomes during immunotherapy, the gut microbiome is only one of many factors that influence the efficacy of treatment. Some individuals, despite having a ‘healthy’ gut microbiome, will not respond to ICIs; this is also evident from recent phase I FMT trials in refractory patients with melanoma<sup>59,60</sup>. This suggests that modulating the microbiome via diet, FMT or probiotics and antibiotics to induce an immune and microbiome landscape that is more conducive to response will be of clinical benefit to those patients whose tumors are intrinsically capable of responding. Personalized approaches guided by an individual’s microbiome will probably be necessary to optimize the utility of microbial interventions, along with integration with other tumor-intrinsic and tumor-extrinsic factors.

We analyzed gut microbiota composition and diet, and their associations with ICI treatment outcomes, in patients from three countries on different continents. Notably, the study uses a large prospective homogeneous cohort of patients with stage III melanoma enrolled in clinical trials in Australia and the Netherlands. The findings highlight that despite the clinical homogeneity of the cohort, individual taxa are not generalizable predictors of clinical outcomes. Exploring the biology underpinning the differences between cohorts and their association with response, we found that diet-driven microbial ecology underpins associations between gut microbes and clinical outcomes and may help to explain discordant findings of previous studies<sup>18–20</sup>. Critically, we show that *Ruminococcaceae*-dominated microbiomes are beneficial in facilitating responses to immunotherapy and emphasize that a fiber-imprinted microbiome in isolation is not sufficient to induce a response. Overall, our data demonstrate a path to optimizing the utility of the microbiome in the clinic and development of more targeted interventions to reshape the microbiome and improve treatment outcomes.

## Online content

Any methods, additional references, Nature Research reporting summaries, source data, extended data, supplementary information, acknowledgements, peer review information; details of author contributions and competing interests; and statements of data and code availability are available at <https://doi.org/10.1038/s41591-022-01965-2>.

Received: 3 May 2022; Accepted: 22 July 2022;

Published online: 22 September 2022

## References

- Seidel, J. A., Otsuka, A. & Kabashima, K. Anti-PD-1 and anti-CTLA-4 therapies in cancer: mechanisms of action, efficacy, and limitations. *Front Oncol.* **8**, 86 (2018).
- Larkin, J. et al. Five-year survival with combined nivolumab and ipilimumab in advanced melanoma. *N. Engl. J. Med.* **381**, 1535–1546 (2019).
- Larkin, J. et al. Combined nivolumab and ipilimumab or monotherapy in untreated melanoma. *N. Engl. J. Med.* **373**, 23–34 (2015).
- Wolchok, J. D. et al. Overall survival with combined nivolumab and ipilimumab in advanced melanoma. *N. Engl. J. Med.* **377**, 1345–1356 (2017).
- Long, G. V. et al. Standard-dose pembrolizumab in combination with reduced-dose ipilimumab for patients with advanced melanoma (KEYNOTE-029): an open-label, phase 1b trial. *Lancet Oncol.* **18**, 1202–1210 (2017).

6. Long, G. V. et al. Combination nivolumab and ipilimumab or nivolumab alone in melanoma brain metastases: a multicentre randomised phase 2 study. *Lancet Oncol.* **19**, 672–681 (2018).
7. Rozeman, E. A. et al. Identification of the optimal combination dosing schedule of neoadjuvant ipilimumab plus nivolumab in macroscopic stage III melanoma (OpACIN-neo): a multicentre, phase 2, randomised, controlled trial. *Lancet Oncol.* **20**, 948–960 (2019).
8. Menzies, A. M. et al. Pathological response and survival with neoadjuvant therapy in melanoma: a pooled analysis from the International Neoadjuvant Melanoma Consortium (INMC). *Nat. Med.* **27**, 301–309 (2021).
9. Rozeman, E. A. et al. Survival and biomarker analyses from the OpACIN-neo and OpACIN neoadjuvant immunotherapy trials in stage III melanoma. *Nat. Med.* **27**, 256–263 (2021).
10. Luke, J. J., Flaherty, K. T., Ribas, A. & Long, G. V. Targeted agents and immunotherapies: optimizing outcomes in melanoma. *Nat. Rev. Clin. Oncol.* **14**, 463–482 (2017).
11. Grainger, J., Daw, R. & Wemyss, K. Systemic instruction of cell-mediated immunity by the intestinal microbiome. *F1000Res* **7**, (2018).
12. Harkiolaki, M. et al. T cell-mediated autoimmune disease due to low-affinity crossreactivity to common microbial peptides. *Immunity* **30**, 348–357 (2009).
13. Horai, R. et al. Microbiota-dependent activation of an autoreactive t cell receptor provokes autoimmunity in an immunologically privileged site. *Immunity* **43**, 343–353 (2015).
14. Parada Venegas, D. et al. Short chain fatty acids (scfas)-mediated gut epithelial and immune regulation and its relevance for inflammatory bowel diseases. *Front Immunol.* **10**, 277 (2019).
15. Steed, A. L. et al. The microbial metabolite desaminotyrosine protects from influenza through type I interferon. *Science* **357**, 498–502 (2017).
16. Bachem, A. et al. Microbiota-derived short-chain fatty acids promote the memory potential of antigen-activated CD8(+) T cells. *Immunity* **51**(2), 285–297.e5, <https://doi.org/10.1016/j.immuni.2019.06.002> (2019).
17. Marchesi, J. R. et al. The gut microbiota and host health: a new clinical frontier. *Gut* **65**, 330–339 (2016).
18. Matson, V. et al. The commensal microbiome is associated with anti-PD-1 efficacy in metastatic melanoma patients. *Science* **359**, 104–108 (2018).
19. Gopalakrishnan, V. et al. Gut microbiome modulates response to anti-PD-1 immunotherapy in melanoma patients. *Science* **359**, 97–103 (2018).
20. Routy, B. et al. Gut microbiome influences efficacy of PD-1-based immunotherapy against epithelial tumors. *Science* **359**, 91–97 (2018).
21. Vétizou, M. et al. Anticancer immunotherapy by CTLA-4 blockade relies on the gut microbiota. *Science* **350**, 1079–1084 (2015).
22. Chaput, N. et al. Baseline gut microbiota predicts clinical response and colitis in metastatic melanoma patients treated with ipilimumab. *Ann. Oncol.* **28**, 1368–1379 (2017).
23. Coutzac, C. et al. Systemic short chain fatty acids limit antitumor effect of CTLA-4 blockade in hosts with cancer. *Nat. Commun.* **11**, 2168 (2020).
24. Smith, M. et al. Gut microbiome correlates of response and toxicity following anti-CD19 CAR T cell therapy. *Nat. Med.* **28**, 713–723 (2022).
25. Andrews, M. C. et al. Gut microbiota signatures are associated with toxicity to combined CTLA-4 and PD-1 blockade. *Nat. Med.* **27**, 1432–1441 (2021).
26. McCulloch, J. A. et al. Intestinal microbiota signatures of clinical response and immune-related adverse events in melanoma patients treated with anti-PD-1. *Nat. Med.* **28**, 545–556, <https://doi.org/10.1038/s41591-022-01698-2> (2022).
27. Lee, K. A. et al. Cross-cohort gut microbiome associations with immune checkpoint inhibitor response in advanced melanoma. *Nat. Med.* **28**, 535–544, <https://doi.org/10.1038/s41591-022-01695-5> (2022).
28. Ghabraibeh, R. Z. & Jobin, C. Microbiota and cancer immunotherapy: in search of microbial signals. *Gut* **68**, 385–388, <https://doi.org/10.1136/gutjnl-2018-317220> (2018).
29. Tetzlaff, M. T. et al. Pathological assessment of resection specimens after neoadjuvant therapy for metastatic melanoma. *Ann. Oncol.* **29**, 1861–1868 (2018).
30. Amaria, R. N. et al. Neadjuvant systemic therapy in melanoma: recommendations of the International Neoadjuvant Melanoma Consortium. *Lancet Oncol.* **20**, e378–e389 (2019).
31. Frankel, A. E. et al. Metagenomic shotgun sequencing and unbiased metabolomic profiling identify specific human gut microbiota and metabolites associated with immune checkpoint therapy efficacy in melanoma patients. *Neoplasia* **19**, 848–855 (2017).
32. Peters, B. A. et al. Relating the gut metagenome and metatranscriptome to immunotherapy responses in melanoma patients. *Genome Med* **11**, 61 (2019).
33. Yu, L. C. Microbiota dysbiosis and barrier dysfunction in inflammatory bowel disease and colorectal cancers: exploring a common ground hypothesis. *J. Biomed. Sci.* **25**, 79 (2018).
34. Rajca, S. et al. Alterations in the intestinal microbiome (dysbiosis) as a predictor of relapse after infliximab withdrawal in Crohn's disease. *Inflamm. Bowel Dis.* **20**, 978–986 (2014).
35. Bang, C. & Schmitz, R. A. Archaea associated with human surfaces: not to be underestimated. *FEMS Microbiol. Rev.* **39**, 631–648 (2015).
36. Smith, N. W., Shorten, P. R., Altermann, E. H., Roy, N. C. & McNabb, W. C. Hydrogen cross-feeders of the human gastrointestinal tract. *Gut Microbes* **10**, 270–288 (2019).
37. Belkaid, Y. & Hand, T. W. Role of the microbiota in immunity and inflammation. *Cell* **157**, 121–141 (2014).
38. Llewellyn, S. R. et al. Interactions between diet and the intestinal microbiota alter intestinal permeability and colitis severity in mice. *Gastroenterology* **154**, e1032 (2018).
39. Nestel, P. et al. Indications for omega-3 long chain polyunsaturated fatty acid in the prevention and treatment of cardiovascular disease. *Heart Lung Circ.* **24**, 769–779 (2015).
40. Macia, L. et al. Metabolite-sensing receptors GPR43 and GPR109A facilitate dietary fibre-induced gut homeostasis through regulation of the inflammasome. *Nat. Commun.* **6**, 6734 (2015).
41. Chiba, M., Nakane, K. & Komatsu, M. Westernized diet is the most ubiquitous environmental factor in inflammatory bowel disease. *Perm. J.* **23**, 18–107 (2019).
42. Watson, H. et al. A randomised trial of the effect of omega-3 polyunsaturated fatty acid supplements on the human intestinal microbiota. *Gut* **67**, 1974–1983 (2018).
43. Lam, Y. Y. et al. Effects of dietary fat profile on gut permeability and microbiota and their relationships with metabolic changes in mice. *Obes. (Silver Spring)* **23**, 1429–1439 (2015).
44. Mager, L. F. et al. Microbiome-derived inosine modulates response to checkpoint inhibitor immunotherapy. *Science* **369**, 1481–1489 (2020).
45. Dubin, K. et al. Intestinal microbiome analyses identify melanoma patients at risk for checkpoint-blockade-induced colitis. *Nat. Commun.* **7**, 10391 (2016).
46. Chen, J., Zhao, K.N. & Vitetta, L. Effects of intestinal microbial(-)elaborated butyrate on oncogenic signaling pathways. *Nutrients* **11**(5), 1026 (2019).
47. He, Y. et al. Regional variation limits applications of healthy gut microbiome reference ranges and disease models. *Nat. Med.* **24**, 1532–1535 (2018).
48. Arumugam, M. et al. Enterotypes of the human gut microbiome. *Nature* **473**, 174–180 (2011).
49. Holmes, I., Harris, K. & Quince, C. Dirichlet multinomial mixtures: generative models for microbial metagenomics. *PLoS One* **7**, e30126 (2012).
50. Wu, G. D. et al. Linking long-term dietary patterns with gut microbial enterotypes. *Science* **334**, 105–108 (2011).
51. Costea, P. I. et al. Enterotypes in the landscape of gut microbial community composition. *Nat. Microbiol* **3**, 8–16 (2018).
52. Singh, R. K. et al. Influence of diet on the gut microbiome and implications for human health. *J. Transl. Med* **15**, 73 (2017).
53. Chung, D. & Keles, S. Sparse partial least squares classification for high dimensional data. *Stat Appl Genet Mol Biol* **9**(1), (2010).
54. Spencer, C. N. et al. Dietary fiber and probiotics influence the gut microbiome and melanoma immunotherapy response. *Science* **374**, 1632–1640 (2021).
55. Kovatcheva-Datchary, P. et al. Dietary fiber-induced improvement in glucose metabolism is associated with increased abundance of prevotella. *Cell Metab.* **22**, 971–982 (2015).
56. Zeevi, D. et al. Personalized nutrition by prediction of glycemic responses. *Cell* **163**, 1079–1094 (2015).
57. Zmora, N. et al. Personalized gut mucosal colonization resistance to empiric probiotics is associated with unique host and microbiome features. *Cell* **174**, 1388–1405 e1321 (2018).
58. Lam, K. C. et al. Microbiota triggers STING-type I IFN-dependent monocyte reprogramming of the tumor microenvironment. *Cell* <https://doi.org/10.1016/j.cell.2021.09.019> (2021).
59. Baruch, E. N. et al. Fecal microbiota transplant promotes response in immunotherapy-refractory melanoma patients. *Science* **371**(6529), 602–609, <https://doi.org/10.1126/science.abb5920> (2020).
60. Davar, D. et al. Fecal microbiota transplant overcomes resistance to anti-PD-1 therapy in melanoma patients. *Science* **371**, 595–602 (2021).

**Publisher's note** Springer Nature remains neutral with regard to jurisdictional claims in published maps and institutional affiliations.

Springer Nature or its licensor holds exclusive rights to this article under a publishing agreement with the author(s) or other rightsholder(s); author self-archiving of the accepted manuscript version of this article is solely governed by the terms of such publishing agreement and applicable law.

© The Author(s), under exclusive licence to Springer Nature America, Inc. 2022

## Methods

**Study design and participants.** All patients were participants in the investigator-led open-label phase 2 randomized, controlled OpACIN-neo or PRADO extension trials (NCT02977052)<sup>7</sup> who were enrolled at the Melanoma Institute Australia or Netherlands Cancer Institute. The medical ethics review committee of the Netherlands Cancer Institute and ethical committees at the Melanoma Institute Australia approved the trial. The trial was conducted in accordance with the protocols and good clinical practice guidelines of the International Conference on Harmonization and the Declaration of Helsinki. All participating patients provided written informed consent before enrollment. Samples were collected under the Melanoma Institute Australia Biospecimen Bank for Melanoma Research Protocol (X15-0454, HREC/11/RPAH/444), and clinical data were collected under the Melanoma Institute Australia: Melanoma Research Database Protocol (X15-0311, HREC/10/RPAH/530). Analysis was conducted under the Melanoma Institute Australia Molecular Pathology, Genomics and Clinical Outcomes Of Melanoma And Related Skin Tumor Protocol (X17-0312, HREC/11/RPAH/32).

Eligible patients were 18 years or older with cytologically or histologically confirmed resectable stage III melanoma with one or more macroscopic lymph node metastases that were measurable according to the Response Evaluation Criteria in Solid Tumors (RECIST) v1.1 ( $>15$  mm short axis). A WHO performance status of 0 or 1, normal organ function and normal lactate dehydrogenase levels were required. Exclusion criteria included in-transit metastasis within the past 6 months, autoimmune disease, HIV infection, hepatitis B or C infection, previous radiotherapy, previous immunotherapy targeting CTLA-4, PD-1, or PD-L1, or immunosuppressive medication within the 6 months directly prior to study inclusion.

Patient fecal samples were collected at baseline, before treatment with ipilimumab and nivolumab (Bristol-Myers Squibb), over a 6-week period according to the dosing schedule outlined in Supplementary Table 1. All dosing arms were grouped together in this study for increased statistical power.

Patients enrolled in the PRADO extension trial had an index node (largest node involved with melanoma) identified at baseline, and resected at week 6, followed by a therapeutic lymph node dissection on a separate occasion if there was a partial or no pathological response in the index node. Patients enrolled in the OpACIN-neo trial underwent a therapeutic lymph node dissection at week 6, regardless of pathological response. Pathological response was determined by pathologists experienced in judging response upon neoadjuvant checkpoint inhibition in stage III melanoma, using the International Neoadjuvant Melanoma Consortium scoring system<sup>28,29</sup> (complete pathological response, no viable tumor; near-complete pathological response,  $\leq 10\%$  viable tumor compared with baseline tumor bed; partial pathological response,  $\leq 50\%$  viable tumor compared with baseline tumor bed; no pathological response,  $> 50\%$  viable tumor compared with baseline tumor bed).

irAEs were scored according to the NCI Common Terminology Criteria for Adverse Events (CTCAE) 4.0, and immune-relatedness to CICB therapy ('possible', 'probable', 'definite' association) was assigned based on the consensus opinion of at least two independent clinical investigators. irAEs rated as 'probable' or 'definite' were included. Patients were classified based on the highest grade of irAEs experienced, with patients classified as 'severe' if they had at least one serious irAE  $\geq$  grade 3 (G3) (as per<sup>7</sup>). The remaining patients were classified as 'mild' (Supplementary Tables 2 and 3).

**Fecal DNA preparation.** Fecal samples were self-collected using the EasySampler Stool collection kit (GP Medical Devices) according to the manufacturer's instructions. Fecal samples were returned in person, aliquotted and stored at  $-80^{\circ}\text{C}$  within 48 h of collection. DNA was isolated using the FastDNA Spin Kit for Feces (MP Biomedicals) and stored at  $-80^{\circ}\text{C}$ . DNA concentration was measured using the Qubit dsDNA BR assay kit (Invitrogen). Mock preparations covering all steps of the procedure were conducted as contamination process controls.

**16S rRNA gene amplicon sequencing and analysis.** 16S rRNA gene amplicon sequencing was used to classify bacterial and archaeal components of fecal microbiomes. Barcoded amplicon libraries spanning the V4 hypervariable region of the gene encoding 16S rRNA (515F-806R primer set) were prepared, and samples were sequenced using the Illumina MiSeq v2 2  $\times$  250 bp platform at the Ramaciotti Centre for Genomics, University of New South Wales, Sydney, Australia. Raw sequence reads were processed using the DADA2 R package, which involves using error profiles to define ASVs<sup>31</sup>. ASVs were assigned to taxonomy using a pre-trained naïve Bayes classifier trained on the curated 16S rRNA gene database Greengenes v13\_8 (99% OTUs, 515F-806R region). Any ASV that was present in fewer than 5% of samples or that was observed less than 100 observations in total, and ASVs that had less than 0.01% of total reads were filtered from the final dataset prior to downstream analysis. Sequencing depth analyses and rarefaction were performed with the phyloseq R package<sup>32</sup>.

Analysis and graphical presentation of the resultant ASV data were performed in R using the packages *phyloseq*, *vegan*, *microbiome* and *ggplot2*. Alpha-diversity metrics (Inverse Simpson's) were calculated on rarefied ASV counts. Beta diversity was assessed on centered-log-ratio-transformed ASV counts, using Bray-Curtis dissimilarity and principal coordinate plots generated from the resultant dissimilarity matrix. The LEfSe method<sup>33</sup> was used to identify taxa that were most likely to explain differences between groups, using relative abundance (total-sum-scaled) data.

**Microbiome community typing.** Patient microbiomes were stratified into community types using Dirichlet Multinomial Mixtures<sup>48</sup>, based on the filtered ASV table generated above from 16S rRNA gene amplicon sequencing. This method assesses a range of values to determine the optimal number of clusters in the provided dataset. Dominant taxa groups (Ba or Ru) were assigned from family-level relative abundances according to the comparative abundance of *Bacteroidaceae* and *Ruminococcaceae*.

**Metagenomic sequencing.** Metagenomics shotgun sequencing was conducted on fecal samples from the Australian patients enrolled in the OpACIN-neo clinical trial ( $n=38$ ). Metagenomic shotgun sequencing was performed utilizing the same DNA from the same preparations as for the 16S rRNA gene analysis. Individual libraries were prepared using Nextera XT, and sequencing was performed on the Illumina NovaSeq 6000 S1 (2  $\times$  150bp; Xp workflow) at the Ramaciotti Centre for Genomics. An average of 22.2 million reads were generated per sample, ranging from 5.1 to 34.8 million reads (only 3 samples had fewer than 15 million reads). The sequence reads (forward reads) were processed using KneadData (v0.7.2; <http://huttenhower.sph.harvard.edu/kneaddata>) with reads mapping to the human genome and bacterial 16S rRNA genes filtered out from the dataset using the human genome (GRCh37/hg19) and ribosomal RNA (SILVA) databases, respectively. The resultant high-quality reads were then mapped against a database of clade-specific marker sequences to assign reads to microbial clades (taxonomic assignment) using MetaPhlAn2 (ref. <sup>64</sup>). The HUMAnN2 (ref. <sup>65</sup>) pipeline was utilized for functional profiling to identify gene families and metabolic pathways. In brief, using taxonomic profiles identified using MetaPhlAn2, sequence reads were mapped at the nucleotide level to species-specific pan-genome databases (generated from the NCBI microbial reference genome collection), with additional translated searches performed against the UniRef90 (ref. <sup>66</sup>) protein database. Metabolic pathways were mapped based on MetaCyc<sup>67</sup>. Gene family and pathway abundance were calculated based on reads per kilobase and normalized to relative abundance. The LEfSe method<sup>63</sup> was used to determine functional pathways that were most likely to explain differences between groups.

**Quantitative PCR.** Targeted bacterial qPCR reactions were conducted using the KAPA SYBR FAST qPCR Master mix (2X) kit (Kapa Biosystems) according to the manufacturer's protocol. 0.5 ng of DNA template was used for patient samples. All qPCRs were validated in previous publications, and cycling protocols can be found in the publications cited in Table 1. All primers and probes are also listed in Table 1. No template controls were set up across all PCRs conducted. All reactions were run in triplicate on a Lightcycler 480 instrument (Roche).

Taxon-specific standard curves were run in triplicate on each plate, using templates with overhanging sequences prepared by PCR followed by gel purification. Copy number was calculated from DNA concentration using the ThermoFisher Scientific DNA copy number calculator. Overhanging primers consisted of the qPCR primer of choice with an 'overhang' that included the M13 primer sequence (see Table 1). Standards were amplified from participant DNA samples. Serial dilutions of taxa-specific PCR standards were in the range of  $10^2$  to  $10^{10}$  copies. Total taxa-specific gene copies per ng of DNA were calculated for each patient sample and normalized to total DNA yield per mg feces to determine the absolute load of each taxon.

**Table 1 | Quantitative PCR primers**

Target group	Primer name	Sequence (5' to 3')	Ref.
Bacterial 16S rRNA	1114-Forward	CGGCAACGAGCGAACCC	73
	1221--Reverse	CCATTGTAGCACGTGTAGCC	
<i>F. prausnitzii</i>	FPR-2F	GGAGGAAGAAGGTCTCGG	74
	Fprau645R	AATTCGCCTACCTCTGCCT	
<i>Oscillospira</i>	OSCI-RV-Fmod	ACGGTACCCCTGAATAAGCC	75,
	OSC-808mod	TCCCCGCACACCTAGTATTG	76
Cluster IV	Rflbr730F	GGCGGYCTRCTGGCTTT	74
<i>Ruminococcus</i> spp.	Clep866mR	CCAGGTGGATWACTTATTGTGTTAA	
Methanogens	Met630F	GGATTAGATACCSGGTAGT	77
	Met803R	GTTGARTCCAATTAAACCGCA	
<i>Megasphaera</i>	Mega-142F	GATGGGGACAACAGCTGGA	78
	Mega-X	GACTCTTTTGGGTTT	
<i>Alistipes</i>	AlisF	TTAGAGATGGGCAT GCGTTGT	79
	AlisR	TGAATCCTCCGATT	
<i>A. muciniphila</i>	AkkF	CAGCACGTGAAGGTGGGGAC	80
	AkkR	CCTTGCCTGGCTTCAGAT	
<i>B. pullucorum</i>	BpullF	GAGGCAGCAGTGGGGAA	81
	BpullR	TCTTCAGGTACCGTCATTGTT	
<i>Enterobacteriaceae</i>	EbactF	CGTCGCAAGCCAAAGAG	82
	EbactR	TTACCGCGCTGCTGGCAC	
M13	M13-Forward	TGTAAAACGACGCCAGT	
	M13-Reverse	CAGGAAACAGCTATGAC	

**Machine learning.** For machine learning, ASVs that compromised less than 0.05% of total reads were filtered from the final dataset prior to downstream analysis. Data were transformed using centered-log-ratio transformations to account for the compositional nature of microbial sequencing data<sup>68</sup>. Principal component analyses (PCA) and sparse partial least square discriminant analysis (sPLS-DA) were performed using the *mixomics* R package<sup>69</sup>. We determined whether samples exhibited statistically significant clustering by experimental groups as previously described<sup>10</sup>. Briefly, the Aitchison metric (Euclidean distance between centered-log-ratio transformed data) was used to calculate the pairwise distance between all samples. Thereafter, the distributions of within-group and between-group sample distances were contrasted using a one-sided Kolmogorov-Smirnov statistic; if the between-group sample distances exceeds the within-group sample distances, then the groups have statistically significantly different microbiota compositions. *P* values were corrected for multiple comparisons using the Bonferroni method.

To assess model accuracy and generalizability, and make maximal use of available patient data, we employed the ‘leave-one-out-cross-validation’ (LOOCV) methodology to build predictive models with sPLS-DA. The available data were repeatedly partitioned into a ‘training’ portion used in model building and a ‘validation’ portion used to assess model performance. Under LOOCV, each sample was retained as the sole validation portion member exactly once, with all remaining data forming the training portion; hence, all available data were ultimately used (once) in assessing model performance. We employed the Mahalanobis distance when using the model to predict the experimental group (class) of the validation data points. Classification accuracies are reported for each class individually. As the number of samples differed across experimental groups, models were trained to minimize the balanced error rate (the average error rate across classes; each class is equally important) rather than the overall error rate (% of total errors; biased towards larger classes). Note that the error rate is 1 - accuracy. For taxa contributing to signatures that distinguish experimental groups, we report only those that were included in >90% of models built under LOOCV.

The statistical significance of sPLS-DA model classification accuracy was estimated through permutation testing. The available samples were randomly reassigned into classes of equal number and size as the original (unperturbed) data. The sPLS-DA training pipeline (including selecting sPLS-DA parameters for the maximum number of components investigated and the number of features to include in each) was then applied to the permuted data, and the most accurate result recorded. This process was repeated 50 times. The estimated *P* value corresponds to the count of permuted dataset accuracies surpassing that of the real data; 50 replicates yields a *P* value granularity of 0.02.

**Additional datasets.** Data from publicly available 16S rRNA gene sequencing datasets from previous microbiome and immunotherapy studies of patients from the United States<sup>18,19</sup> were used to validate the framework. Additionally, the 16S rRNA gene sequence data and dietary intake data from *n*=31 patients receiving neoadjuvant therapy in the United States<sup>44</sup> were provided by the authors. The 16S dataset from ref. <sup>18</sup> was obtained from The NCBI Sequence Read Archive (SRA) (accession number SRP116709) and data from ref. <sup>19</sup> were obtained from the European Nucleotide Archive (accession number PRJEB22894). Raw 16S sequence reads were combined with our dataset and processed together using the DADA2 R package, as reported above, with forward reads only. Any ASV that was present in fewer than 5% of samples or that was observed less than 100 times in total, and ASVs that compromised less than 0.01% of the total reads were filtered from the final dataset prior to downstream analysis, as per the above ASV analysis pipeline.

**Nuclear magnetic resonance spectroscopy.** Quantitative measurements of butyrate in feces and serum were determined by NMR. Feces were homogenized in deuterium oxide, the homogenate was filtered through a 3-kDa membrane and then metabolites in the filtrate were extracted from the aqueous phase of a deuterium methanol and deuterium chloroform mixture. Serum was prepared for NMR using the same filtration and extraction steps. The samples, containing 4,4-dimethyl-4-silapentane-1-sulfonic acid as an internal standard, were analyzed on a Bruker 600 MHz NMR.

**Nutritional input.** To assess dietary patterns in the Australian patients (*n*=63), nutrient intake data covering a 6 to 12-month period was collected using the Cancer Council Victoria Dietary Questionnaire for Epidemiological Studies (DQES v3.2). Analysis of questionnaires for assessment of dietary intake was undertaken by the Nutritional Assessment Office, Cancer Council Victoria, Australia. The questionnaire covers 80 items across five types of dietary intake: cereals; dairy; meat and fish; fruit; vegetables; and alcoholic beverages. From the dietary intake data, 55 macronutrient and micronutrient intakes are calculated. To assess dietary patterns in the Dutch patients (*n*=32), nutrient intake data were collected using the Food Frequency Questionnaire (FQ18N) developed by Wageningen University and Research<sup>71</sup>. As different food intake surveys were used to calculate nutrient intake for Australian and Dutch patients, dietary results from each country cannot be combined. Nutritional data were analyzed according to clinically defined groups and correlated (Spearman’s Rank) with microbial data. Dietary questionnaires were unable to be completed by a subset of patients.

**Statistical analysis.** Graphs were generated using GraphPad Prism v7. Heatmaps were generated using Clustvis<sup>72</sup>. Significance of univariate comparisons was tested using the Mann-Whitney U test, and multiple pairwise group comparisons were tested using the Kruskal-Wallis test with post-hoc Dunn test in GraphPad Prism v7. *P* values were corrected for multiple comparison testing using the Benjamini-Hochberg method (BH). The Spearman’s rank test was used for linear regression.

**Reporting summary.** Further information on research design is available in the Nature Research Reporting Summary linked to this article.

## Data availability

Sequencing data are available from the European Nucleotide Archive under accession number PRJEB22894 and PRJNA770295. Supporting de-identified metadata have been provided. Publicly available datasets were attained from The NCBI Sequence Read Archive (SRA) under accession number SRP116709 and the European Nucleotide Archive under accession numbers PRJEB22894 and PRJNA770295. Further details, data and code are available upon request from the authors.

## Code availability

No unique software or computational code was created for this study. Implementation of established tools and pipelines are described in the methods.

## References

61. Callahan, B. J. et al. DADA2: High-resolution sample inference from Illumina amplicon data. *Nat. Methods* **13**, 581–583 (2016).
62. McMurdie, J. & Holmes, S. Phyloseq: an R package for reproducible interactive analysis and graphics of microbiome census data. *PLoS One* **8**, e61217 (2013).
63. Segata, N. et al. Metagenomic biomarker discovery and explanation. *Genome Biol.* **12**, R60 (2011).
64. Sidhu, P. et al. Radiological manifestations of immune-related adverse effects observed in patients with melanoma undergoing immunotherapy. *J. Med Imaging Radiat. Oncol.* **61**, 759–766 (2017).
65. Franzosa, E. A. et al. Species-level functional profiling of metagenomes and metatranscriptomes. *Nat. Methods* **15**, 962–968 (2018).
66. Suzek, B. E. et al. UniRef clusters: a comprehensive and scalable alternative for improving sequence similarity searches. *Bioinformatics* **31**, 926–932 (2015).
67. Caspi, R. et al. The MetaCyc database of metabolic pathways and enzymes. *Nucleic Acids Res.* **46**, D633–D639 (2018).
68. Gloor, G. B., Macklaim, J. M., Pawlowsky-Glahn, V. & Egoscue, J. J. Microbiome Datasets Are Compositional: And This Is Not Optional. *Front Microbiol* **8**, 2224 (2017).
69. Rohart, F., Gautier, B., Singh, A. & Le Cao, K. A. mixOmics: An R package for ‘omics feature selection and multiple data integration. *PLoS Comput. Biol.* **13**, e1005752 (2017).
70. Zoll, J. et al. Fecal microbiota transplantation from high caloric-fed donors alters glucose metabolism in recipient mice, independently of adiposity or exercise status. *Am. J. Physiol. Endocrinol. Metab.* **319**, E203–E216 (2020).
71. Siebelink, E., Geelen, A. & de Vries, J. H. Self-reported energy intake by FFQ compared with actual energy intake to maintain body weight in 516 adults. *Br. J. Nutr.* **106**, 274–281 (2011).
72. Metsalu, T. & Vilo, J. ClustVis: a web tool for visualizing clustering of multivariate data using Principal Component Analysis and heatmap. *Nucleic Acids Res.* **43**, W566–W570 (2015).
73. Shanahan, E. R. et al. Influence of cigarette smoking on the human duodenal mucosa-associated microbiota. *Microbiome* **6**, 150 (2018).
74. Ramirez-Farias, C. et al. Effect of inulin on the human gut microbiota: stimulation of *Bifidobacterium adolescentis* and *Faecalibacterium prausnitzii*. *Br. J. Nutr.* **101**, 541–550 (2009).
75. Mackie, R. I. et al. Ecology of uncultivated *Oscillospira* species in the rumen of cattle, sheep, and reindeer as assessed by microscopy and molecular approaches. *Appl. Environ. Microbiol.* **69**, 6808–6815 (2003).
76. Yanagita, K. et al. Flow cytometric sorting, phylogenetic analysis and in situ detection of *Oscillospira guillermorandi*, a large, morphologically conspicuous but uncultured ruminal bacterium. *Int J. Syst. Evol. Microbiol.* **53**, 1609–1614 (2003).
77. Hook, S. E., Northwood, K. S., Wright, A. D. & McBride, B. W. Long-term monensin supplementation does not significantly affect the quantity or diversity of methanogens in the rumen of the lactating dairy cow. *Appl. Environ. Microbiol.* **75**, 374–380 (2009).
78. Ohnishi, A. et al. Development of a 16S rRNA gene primer and PCR-restriction fragment length polymorphism method for rapid detection of members of the genus *Megasphaera* and species-level identification. *Appl. Environ. Microbiol.* **77**, 5533–5535 (2011).
79. Layton, A. et al. Development of *Bacteroides* 16S rRNA gene TaqMan-based real-time PCR assays for estimation of total, human, and bovine fecal pollution in water. *Appl. Environ. Microbiol.* **72**, 4214–4224 (2006).

80. Schneeberger, M. et al. Akkermansia muciniphila inversely correlates with the onset of inflammation, altered adipose tissue metabolism and metabolic disorders during obesity in mice. *Sci. Rep.* **5**, 16643 (2015).
81. & Geirnaert, A. et al. Interindividual differences in response to treatment with butyrate-producing *Butyrivibrio pullicaecorum* 25-3 T studied in an *in vitro* gut model. *FEMS Microbiol Ecol* **91**, (2015).
82. Hermann-Bank, M. L., Skovgaard, K., Stockmarr, A., Larsen, N. & Molbak, L. The Gut Microbiotassay: a high-throughput qPCR approach combinable with next generation sequencing to study gut microbial diversity. *BMC Genomics* **14**, 788 (2013).

## Acknowledgements

We thank G. Giles of the Cancer Epidemiology Division, Cancer Council Victoria, for permission to use the Cancer Council Victoria Dietary Questionnaire for Epidemiological Studies (DQES v3.2), Melbourne, Australia, 1996. We acknowledge the technical assistance provided by the Sydney Informatics Hub, a core research facility of the University of Sydney. G.V.L. and R.A.S are supported by NHMRC Program Grant R.A.S is supported by an NHMRC Practitioner Fellowship and G.V.L by an NHMRC Investigator Grant. G.V.L is also supported by the University of Sydney Medical Foundation. Support from the Cameron Family and Ainsworth Foundation, as well as from colleagues at Melanoma Institute Australia, Royal Prince Alfred Hospital and NSW Health Pathology is gratefully acknowledged. E.R.S. acknowledges financial support from The William Arthur Martin a Beckett Cancer Research Trust (University of Sydney Fellowship). Funding support was provided by a Tour de Cure Australia project grant (RSP-00054-19/20) (R.A.S, M.B., E.R.S).

## Author contributions

G.V.L., R.A.S., R.C.S., E.R.S. and M.B. conceived the study. R.C.S., E.R.S., M.B., M.R., A.S.A., J.T., I.L.M.R. and J.V. conducted the experiments. R.C.S., E.R.S., M.B. and M.R. analyzed the data. I.P.S., R.R., C.A., A.M.M., R.P.S., M.G., K.R.S., A.J.S., R.V., A.J.L., A.V.D., A.K.M., M.C., A.B., N.J.A., L.M., and A.J.H. contributed to patient recruitment, biospecimen processing, data analysis and/or critical review of data. J.A.W., C.U.B.,

R.A.S. and G.V.L. contributed resources to the study. R.C.S., E.R.S. and M.B. wrote the original manuscript draft. All authors wrote, reviewed and edited the manuscript. G.V.L., R.A.S. and J.S.W. supervised the study. G.V.L., R.A.S., M.B. and E.R.S. obtained funding for the study.

## Competing interests

A.M.M has received fees for advisory board membership from BMS, MSD, Novartis, Roche, Pierre Fabre and Qbiotics. R.P.M.S. has received honoraria for advisory board participation from MSD, Novartis and Qbiotics, and speaking honoraria from BMS and Novartis. A.J.S has received fees for professional services from Eli Lilly Australia. G.V.L. is a consultant advisor for Agenus, Amgen, Array Biopharma, Boehringer Ingelheim International GmbH, Bristol-Myers Squibb, Evaxion Biotec, Hexal AG (Sandoz Company), Highlight Therapeutics S.L., Innovent Biologics USA, Merck Sharpe and Dohme, Novartis, OncoSec, PHMR Limited, Pierre Fabre, Provecutus, Qbiotics and Regeneron. R.A.S has fees for professional services from Roche, Evaxion, Provecutus Biopharmaceuticals Australia, Qbiotics, Novartis, Merck Sharp and Dohme, NeraCare, AMGEN, Bristol-Myers Squibb, Myriad Genetics and GlaxoSmithKline. All compensation was provided for work completed outside of the current work. The remaining authors declare no competing interests.

## Additional information

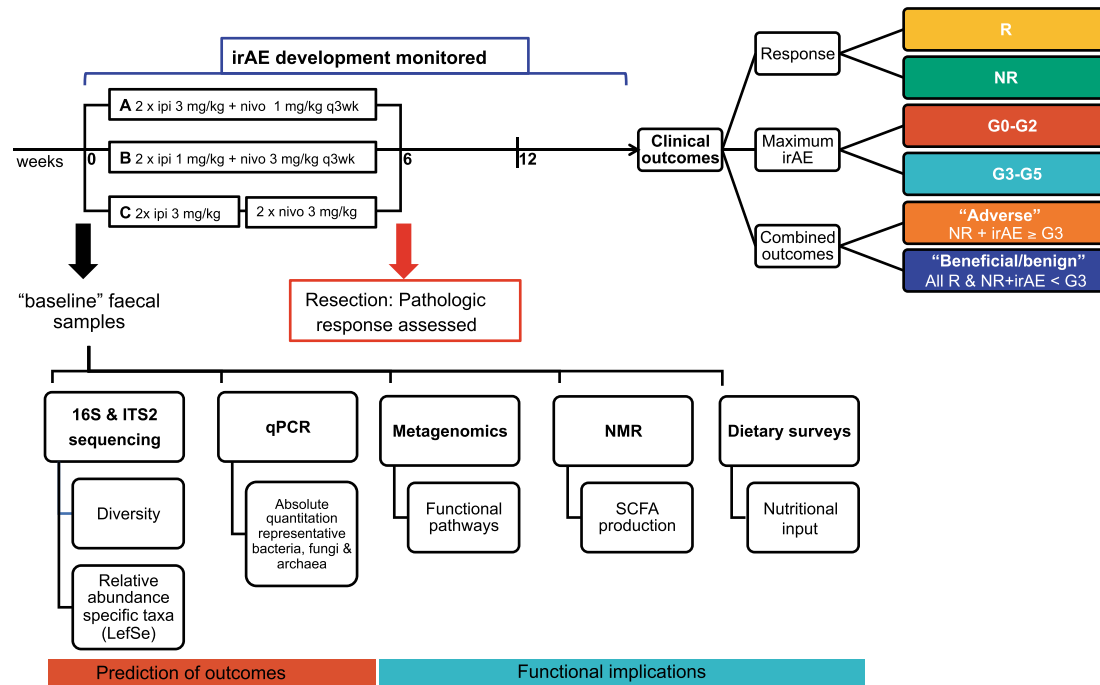
**Extended data** is available for this paper at <https://doi.org/10.1038/s41591-022-01965-2>.

**Supplementary information** The online version contains supplementary material available at <https://doi.org/10.1038/s41591-022-01965-2>.

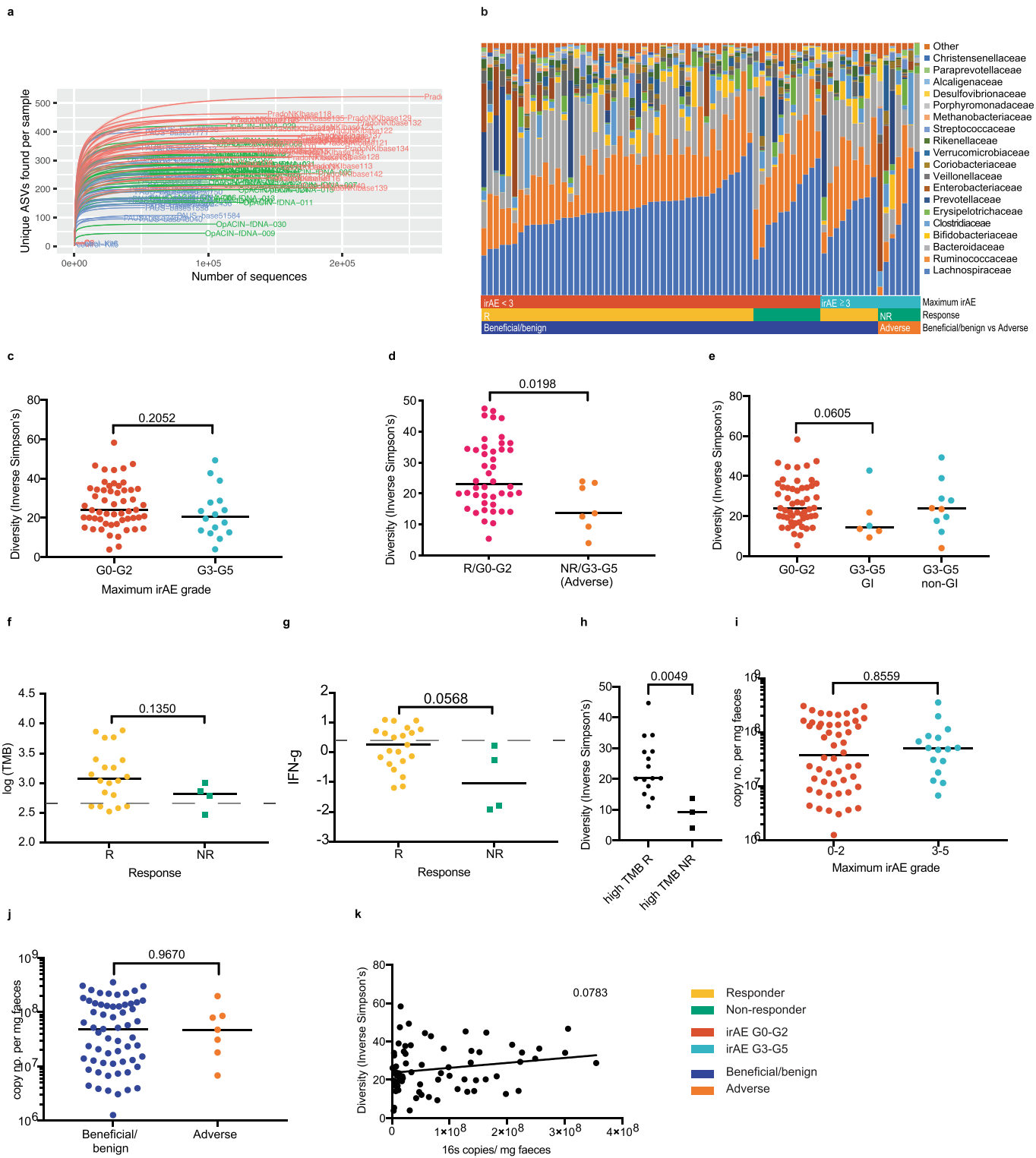
**Correspondence and requests for materials** should be addressed to Georgina V. Long.

**Peer review information** *Nature Medicine* thanks the anonymous reviewers for their contribution to the peer review of this work. Primary Handling Editors: Javier Carmona and Joao Monteiro, in collaboration with the *Nature Medicine* team.

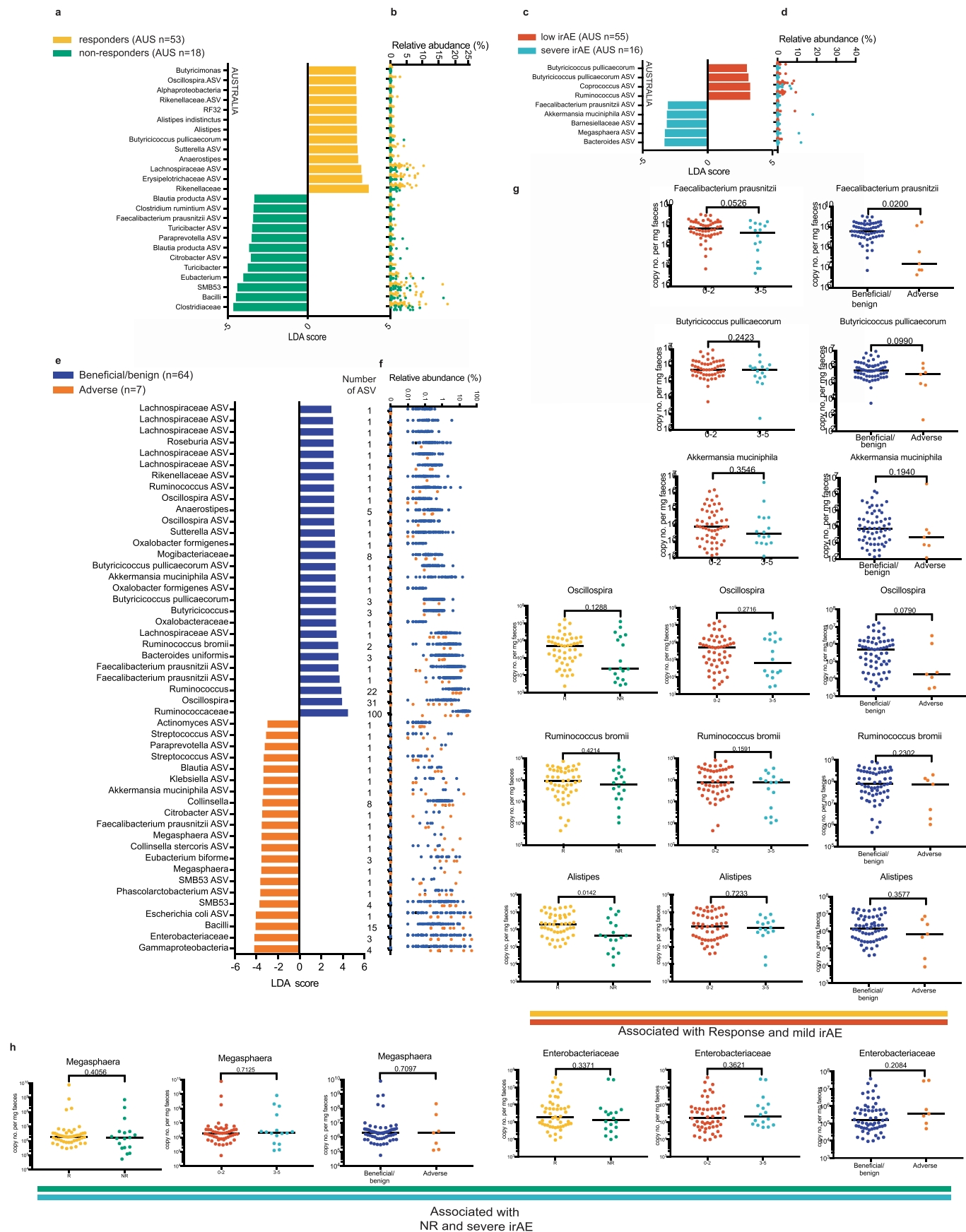
**Reprints and permissions information** is available at [www.nature.com/reprints](http://www.nature.com/reprints).



**Extended Data Fig. 1 |** Cohort and project schematic outlining clinical trial timeline and analyses conducted at baseline.

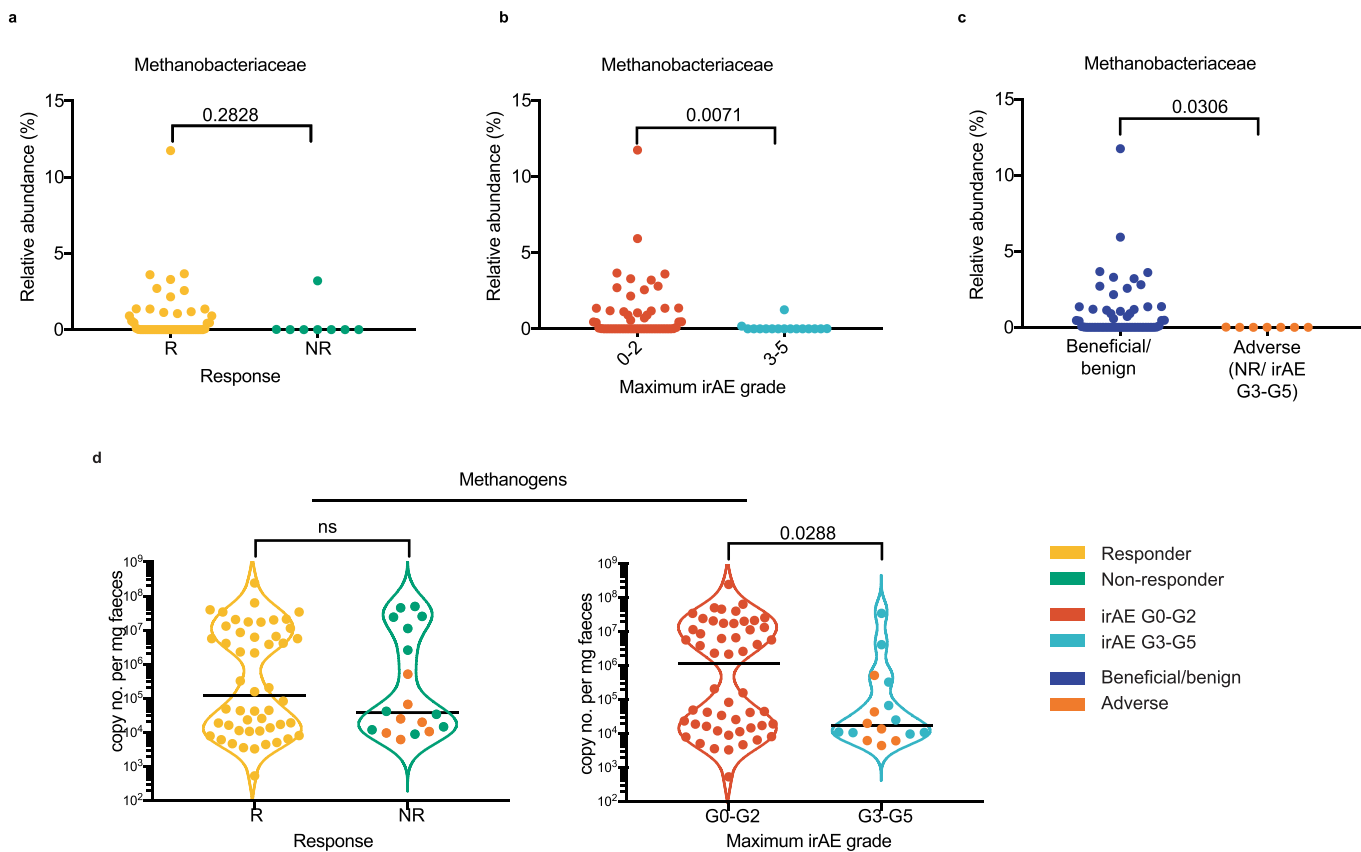


**Extended Data Fig. 2 | (a)** Rarefaction analysis shows sequencing depth was sufficient to comprehensively catalogue the unique microbial strains present. **(b)** Composition of each Australian patient sample classified at the ‘family’ taxonomic level ( $n=71$ ). **(c-e)** Inverse Simpson’s index of alpha diversity for individual patients grouped by **(c)** maximum irAE grade experienced by each patient split by severe irAEs, **(d)** response/low irAE (R/G0-G2) (pink) and non-response/severe irAE (NR) (NR/G3-G5) (orange) or **(e)** maximum irAE grade experienced by each patient split by severe gastrointestinal irAEs and non-gastrointestinal irAEs (NR with severe irAE ‘Adverse’ indicated in orange). (AUS,  $n=7$ ) **(f & g)** Tumour mutational burden (TMB) and tumour IFN-gamma signature split by response. Subset of patients Rozeman et al (2021)<sup>17</sup> ( $n=25$ ). **(h)** Inverse Simpson’s index of alpha diversity for individual patients with high TMB grouped by response and non-response. **(i-j)** Absolute bacterial/archaeal faecal loads assessed using qPCR, with patients grouped by irAEs and ‘Adverse’ outcome groups ( $n=71$ ). **(k)** Correlation of diversity with 16 S rRNA gene number/mg faeces for each patient ( $n=71$ ). Each symbol represents an individual patient, bars indicate the median. Mann-Whitney U rank sum test (c-j). For linear regressions,  $p$  value was calculated on Spearman’s rank correlation (k). All statistical tests are two-sided where appropriate.

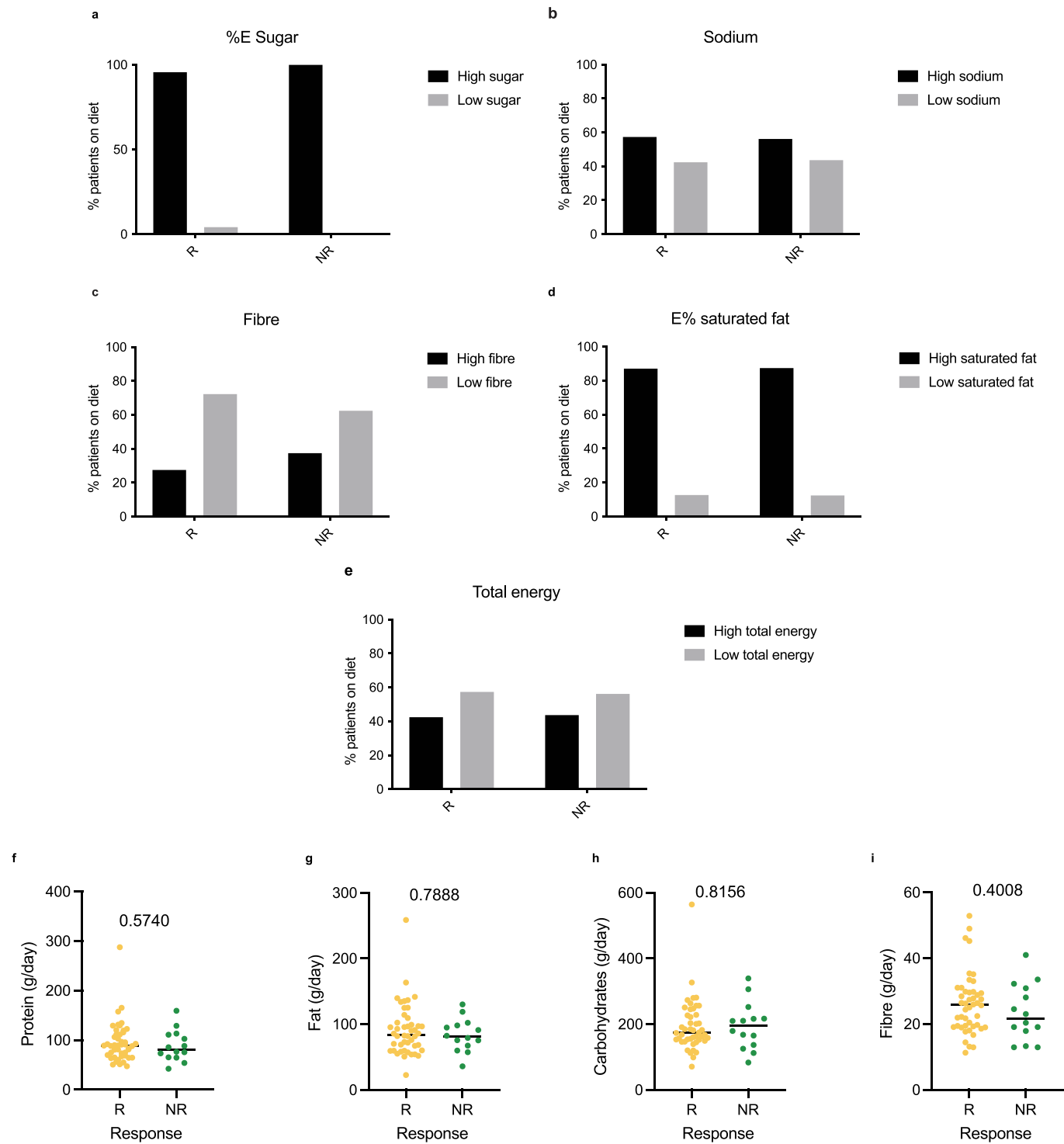


Extended Data Fig. 3 | See next page for caption.

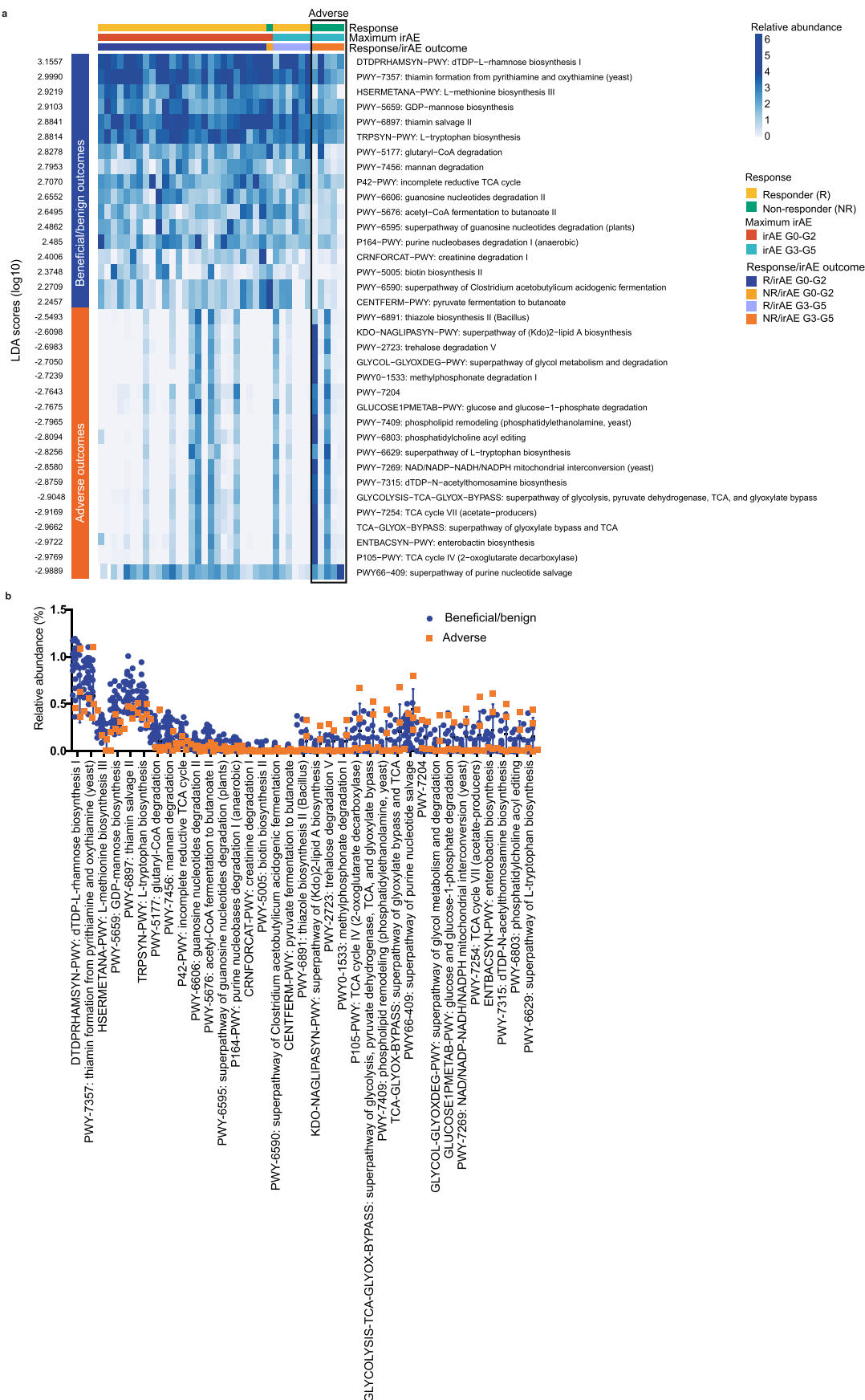
**Extended Data Fig. 3 | (a-f)** Linear discriminant analysis (LDA) scores for differentially abundant taxa in **(a)** response, **(c)** irAE or **(e)** ‘Benefical/benign’ and ‘Adverse’ outcome groupings, as determined by LEfSe analysis (Australian cohort n=71). LDA score indicates the confidence of the association,  $p < 0.05$  for the Kruskal-Wallis H statistic, LDA score  $>3$ . **(b, d & f)** Dot plots show the relative abundance of sequence reads corresponding to each taxa for individual patients, where each dot represents a patient, colours correspond to the legend as indicated. **(g-h)** Quantitative PCR using taxa specific primers was used to determine bacterial copy number per mg faecal matter grouped according to response, irAEs and ‘Adverse’ outcome groups (n=71). **(g)** Taxa associated with response or mild irAE based off LEfSe analysis **(h)** taxa associated with non-response or severe irAE. Each symbol represents an individual patient, bars indicate the median. Mann-Whitney *U* rank sum test (g-h). All statistical tests are two-sided where appropriate.



**Extended Data Fig. 4 | (a-c)** Archaeal ASV in pre-treatment faecal samples were classified using 16 S rRNA gene sequencing. Relative abundance of Archaeal ASVs (*Methanobacteriaceae*) from 16 S rRNA amplicon sequencing was compared by response, maximum irAE grade and ‘Beneficial/benign’ vs ‘Adverse’ outcomes ( $n=71$ ). **(d)** Quantitative PCR on faecal DNA using methanogen specific primers, grouped by response (left) or maximum irAE grade (right) (‘Adverse’ patients are indicated in orange). Each symbol represents an individual patient, bars indicate the median. Mann-Whitney U rank sum test (a-d). All statistical tests are two-sided where appropriate.

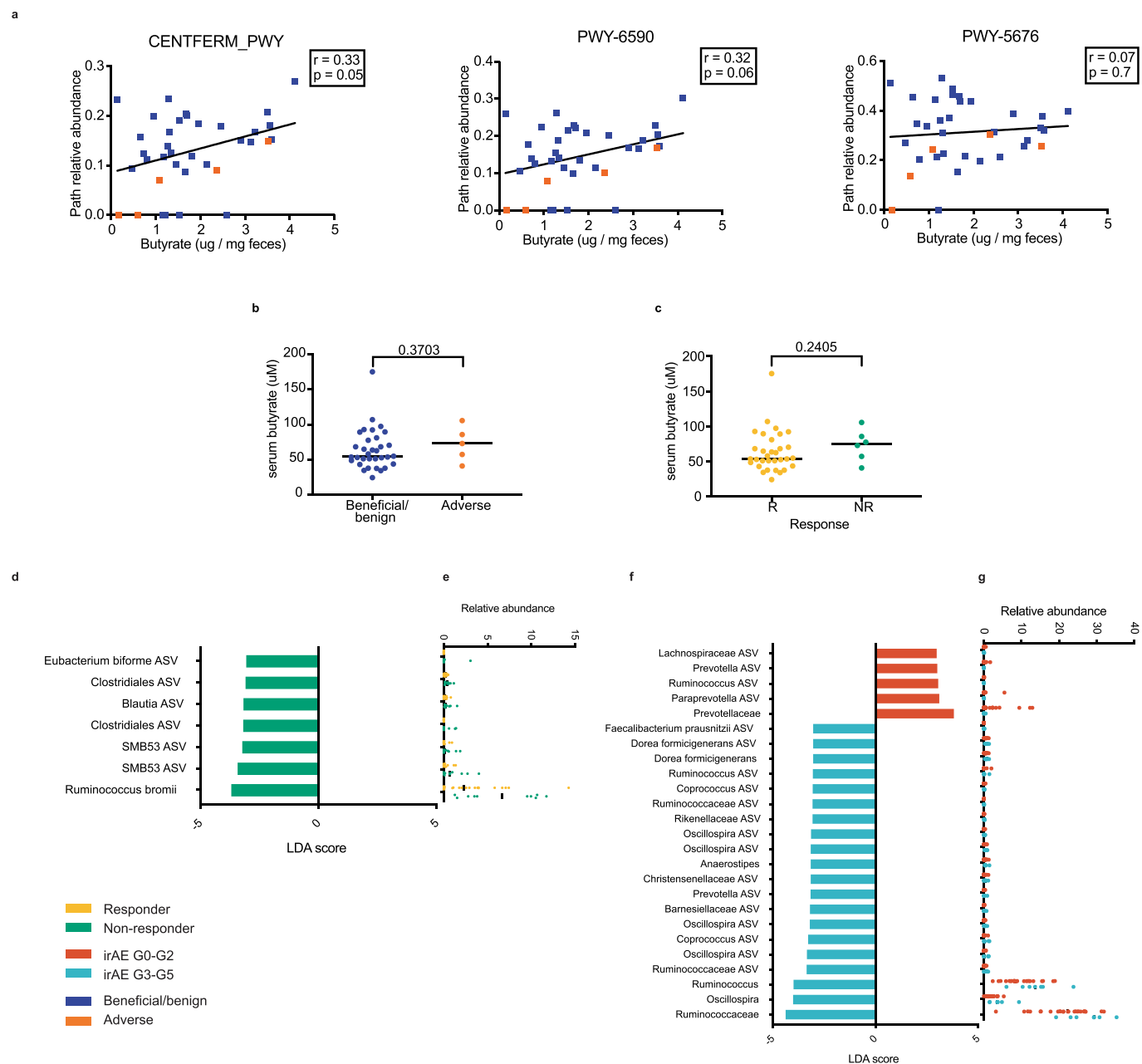


**Extended Data Fig. 5 | (a-e)** Consumption of key dietary nutrients were estimated from food intake surveys. Patients were categorised as low or high according to the Australian dietary recommendations and grouped according to response. **(f-i)** Estimated total **(f)** protein (g/day), **(g)** fat (g/day), **(h)** carbohydrates (g/day) and **(i)** fibre (g/day) consumption from dietary surveys of food intake grouped by response (responder=R (yellow), non-responder=NR (green)) (AUS, n=63). Each symbol represents an individual patient, bars indicate the median. Mann-Whitney U rank test (f-i). All statistical tests are two-sided where appropriate.

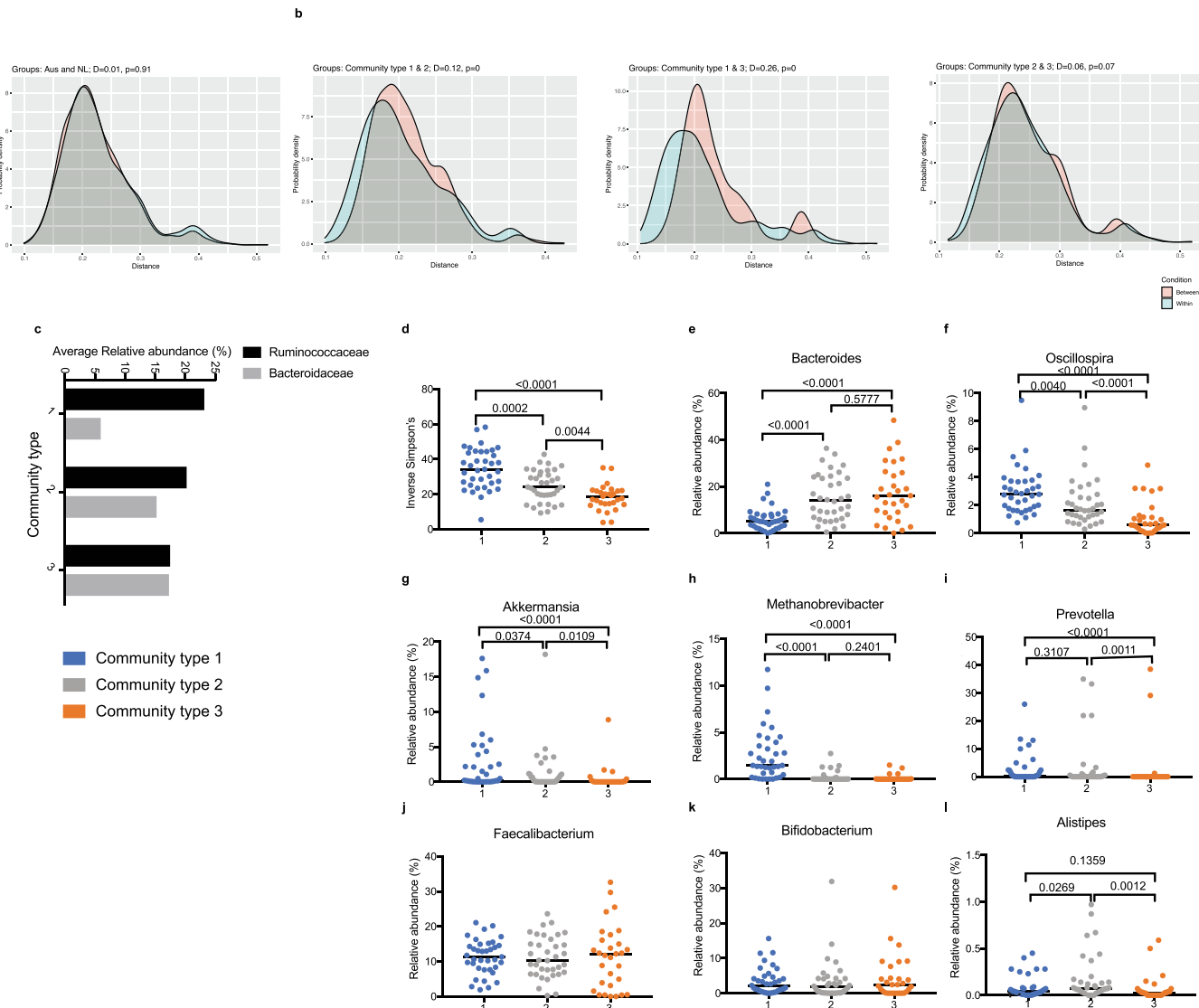


Extended Data Fig. 6 | See next page for caption.

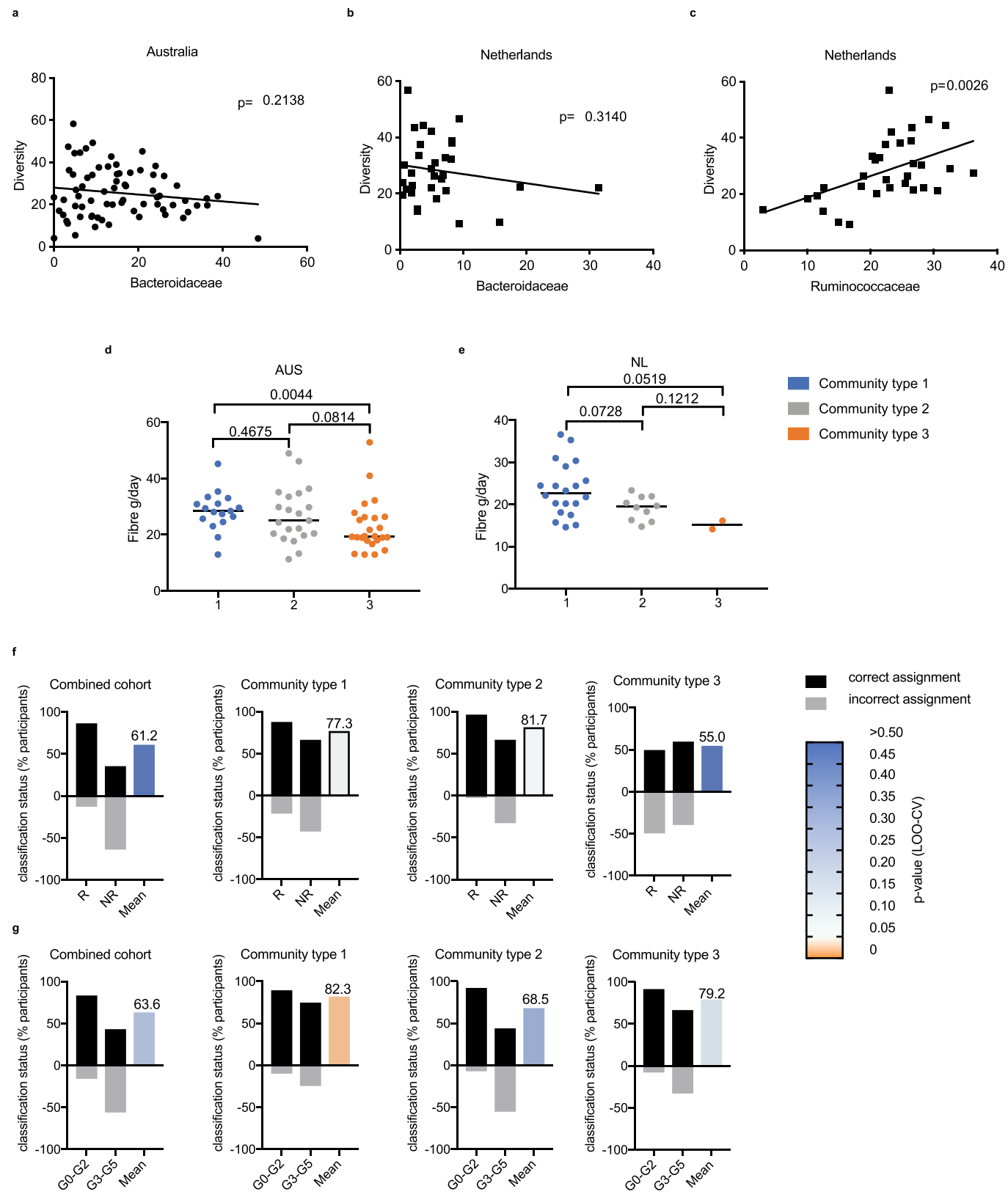
**Extended Data Fig. 6 | (a)** MetaCyc pathways were predicted in the metagenomes of faecal samples of a subset of 38 Australian patients. Linear discriminant analysis (LDA) scores for differentially abundant pathway in the ‘Beneficial/benign’ (all R or NR irAE < G3) verses ‘Adverse’ (NR, irAE $\geq$ 3) outcome group was determined by LEfSe analysis. LDA (log10) score on the left-hand side of the panel indicates the confidence of the association. The heat map indicates relative abundance (%) of each outcome-associated pathway in individual patients. Clinical groupings are indicated by coloured bars at the top. **(b)** Dot plots show the relative abundance of metabolic pathways identified by LEfSe analysis as indicative of ‘Beneficial/benign’ or ‘Adverse’ outcome groups, where each dot represents a patient (subset of Australian cohort n=38).



**Extended Data Fig. 7 | (a)** Correlation of the relative abundance of outcome-associated butyrate pathways (metagenomic data) versus faecal butyrate concentrations, as assessed by NMR. For linear regressions,  $p$  values were calculated on Spearman's rank correlation. **(b-c)** Serum butyrate levels ( $\mu\text{M}$ ) detecting using NMR grouped according to **(b)** 'Beneficial/benign' or 'Adverse' outcome or **(c)** response groupings (subset AUS,  $n=38$ ). Mann-Whitney  $U$  rank test. **(d-g)** Linear discriminant analysis (LDA) scores for differentially abundant taxa in **(d)** response and **(f)** irAE groupings (Dutch cohort,  $n=32$ ), as determined by LEfSe analysis. LDA score indicates the confidence of the association,  $p < 0.05$  for the Kruskal-Wallis  $H$  statistic, LDA score  $>3$ . **(e & g)** Dot plots show the relative abundance of sequence reads corresponding to each taxa for individual patients, where each dot represents a patient. All statistical tests are two-sided where appropriate.

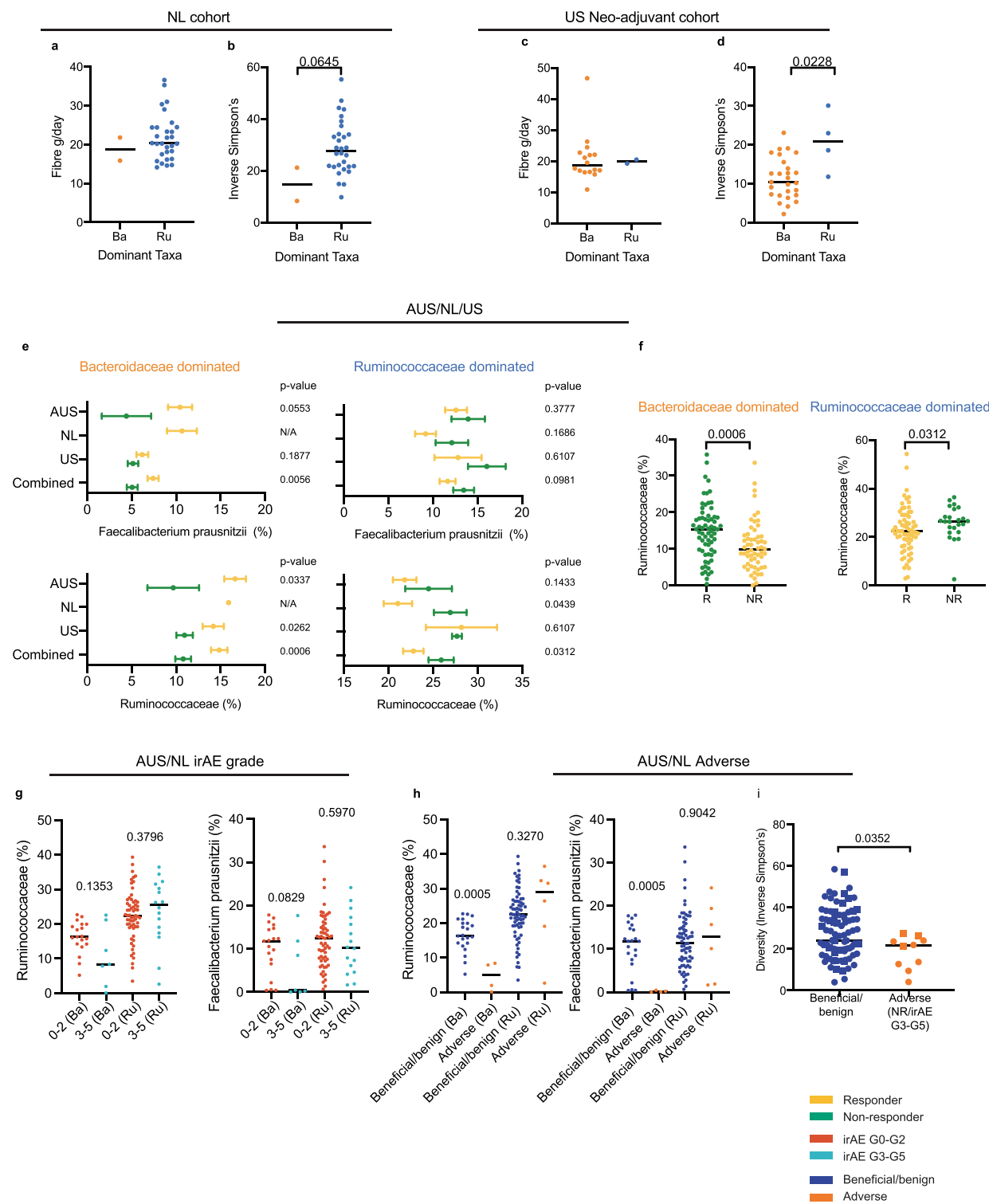


**Extended Data Fig. 8 | (a-b)** Assessing clustering of samples **(a)** by country or **(b)** by DMM community type (combined AUS & NL, n=103), by contrasting distances between samples within the same groups and between groups; distribution of distances shown. Significance assessed through the Kolmogorov-Smirnov statistic (D = effect magnitude value); p-values were corrected for multiple comparisons using the Bonferroni method. **(c)** Average relative abundance of *Bacteroidaceae* and *Ruminococcaceae* per community type. **(d)** Inverse Simpson's index of alpha diversity for individual patients grouped by DMM community type (combined AUS & NL, n=103). Each symbol represents an individual patient, bars indicate the median. **(e-l)** Relative abundance of genus level taxa by DMM community type (combined AUS & NL, n=103). Each symbol represents an individual patient, bars indicate the median. Kruskal-Wallis with post hoc Dunn test. FDR adjusted p-values presented (d-l). All statistical tests are two-sided where appropriate.



Extended Data Fig. 9 | See next page for caption.

**Extended Data Fig. 9 | (a)** Correlation between *Bacteroidaceae* with Diversity in the Australian cohort ( $n=71$ ). **(b-c)** Correlation between **(b)** *Bacteroidaceae* or **(c)** *Ruminococcaceae* with Diversity in the Dutch cohort ( $n=32$ ). Each symbol represents an individual patient. For linear regressions, p value was calculated on Spearman's rank correlation. **(d-e)** Estimated fibre consumption (g/day) from food intake surveys for **(d)** Australian ( $n=63$ ) and **(e)** Dutch patients ( $n=32$ ), grouped by DMM community type. Each symbol represents an individual patient, bars indicate the median. Mann-Whitney U rank sum test. **(f-g)** Baseline microbial signatures that distinguish patient outcomes ('classes') were determined based on microbial variables through sparse partial least squares discriminant analysis (sPLS-DA). Models were constructed from 16S rRNA gene profiles to discriminate **(f)** responders (R) and non-responders (NR) to immunotherapy and **(g)** absent/mild (G0-G2) and severe (G3-G5) irAE development. Models were developed for the combined cohort ( $n=103$ ) and per community type: community type 1 ( $n=37$ ); community type 2 ( $n=36$ ) and community type 3 ( $n=30$ ). Classes are not equally populous; thus, plots depict the classification accuracy per class, with the percentage correctly assigned in black and the mean across classes. Colours indicate p-values derived under permutation testing. All statistical tests are two-sided where appropriate.



**Extended Data Fig. 10 | (a-d)** Estimated fibre (g/day) from food intake surveys and Inverse Simpson diversity grouped by dominant taxa grouping (NL cohort ( $n=32$ ) & US neo-adjuvant cohort (Spencer et al  $n=31$ ). **(e)** Relative abundance of *Faecalibacterium prausnitzii* (top) or *Ruminococcaceae* (bottom), for patients by response (R vs NR) with in dominant taxa groups (Ba & Ru) (presented by country and combined  $n=218$ ). Symbols indicate mean, bars indicate standard error **(f)** Relative abundance of *Ruminococcaceae*, for individual patients within dominant taxa groups (Ba & Ru) by response (combined AUS/NL/US,  $n=218$ ). **(g-h)** Relative abundance of *Ruminococcaceae* (left) or *Faecalibacterium prausnitzii* (right) for patients by **(g)** maximum irAE grade (G0-G2 vs G3-G5) or **(h)** 'Beneficial/benign' (all R or NR irAE  $<$  G3) and 'Adverse' (NR, irAE  $\geq$  G3) outcomes (AUS/N,  $n=103$ ). **(i)** Inverse Simpson's index of alpha diversity for individual patients grouped by 'Beneficial/benign' versus 'Adverse' outcome groups ( $n=103$ , AUS circle, NL square). Each symbol represents an individual patient, bars indicate the median. Mann-Whitney U rank sum test (a-i). All statistical tests are two-sided where appropriate.

## Reporting Summary

Nature Research wishes to improve the reproducibility of the work that we publish. This form provides structure for consistency and transparency in reporting. For further information on Nature Research policies, see our [Editorial Policies](#) and the [Editorial Policy Checklist](#).

### Statistics

For all statistical analyses, confirm that the following items are present in the figure legend, table legend, main text, or Methods section.

n/a Confirmed

- The exact sample size ( $n$ ) for each experimental group/condition, given as a discrete number and unit of measurement
- A statement on whether measurements were taken from distinct samples or whether the same sample was measured repeatedly
- The statistical test(s) used AND whether they are one- or two-sided
  - Only common tests should be described solely by name; describe more complex techniques in the Methods section.*
- A description of all covariates tested
- A description of any assumptions or corrections, such as tests of normality and adjustment for multiple comparisons
- A full description of the statistical parameters including central tendency (e.g. means) or other basic estimates (e.g. regression coefficient) AND variation (e.g. standard deviation) or associated estimates of uncertainty (e.g. confidence intervals)
- For null hypothesis testing, the test statistic (e.g.  $F$ ,  $t$ ,  $r$ ) with confidence intervals, effect sizes, degrees of freedom and  $P$  value noted
  - Give  $P$  values as exact values whenever suitable.*
- For Bayesian analysis, information on the choice of priors and Markov chain Monte Carlo settings
- For hierarchical and complex designs, identification of the appropriate level for tests and full reporting of outcomes
- Estimates of effect sizes (e.g. Cohen's  $d$ , Pearson's  $r$ ), indicating how they were calculated

*Our web collection on [statistics for biologists](#) contains articles on many of the points above.*

### Software and code

Policy information about [availability of computer code](#)

Data collection

Data was collected/collated directly in tabulated form using Microsoft Excel (v16.62) or R (v4.0.5). No custom software was used to collect data in this study

Data analysis

All software and open source code utilized in this study has been previously published and are referenced and described in the methods section.  
General analysis software: R (v4.0.5), Microsoft Excel (v16.62), Prism (v7), ClustVis  
16S sequencing: DADA2, phyloseq, vegan, microbiome, ggplot2, mixomics, DirichletMultinomial, LefSe  
Metagenomic sequencing: KneadData (v0.7.2), MetaPhlAn2, HUMAnN2

For manuscripts utilizing custom algorithms or software that are central to the research but not yet described in published literature, software must be made available to editors and reviewers. We strongly encourage code deposition in a community repository (e.g. GitHub). See the Nature Research [guidelines for submitting code & software](#) for further information.

### Data

Policy information about [availability of data](#)

All manuscripts must include a [data availability statement](#). This statement should provide the following information, where applicable:

- Accession codes, unique identifiers, or web links for publicly available datasets
- A list of figures that have associated raw data
- A description of any restrictions on data availability

Sequence data are deposited in the European Nucleotide Archive with accession number PRJEB54666. Publicly available datasets were attained from The NCBI Sequence Read Archive (SRA) under accession number SRP116709 and the European Nucleotide Archive under accession number PRJEB22894 and PRJNA770295.

Greengenes rDNA database v13\_8 (99% OTUs, 515F-806R region)  
 SILVA rDNA database v138  
 Human genome database (GRCh37/hg19)  
 Species-specific pan-genome databases (NCBI microbial reference genome collection & UniRef90)  
 Metabolic pathways database (MetaCyc)

## Field-specific reporting

Please select the one below that is the best fit for your research. If you are not sure, read the appropriate sections before making your selection.

Life sciences       Behavioural & social sciences       Ecological, evolutionary & environmental sciences

For a reference copy of the document with all sections, see [nature.com/documents/nr-reporting-summary-flat.pdf](https://nature.com/documents/nr-reporting-summary-flat.pdf)

## Life sciences study design

All studies must disclose on these points even when the disclosure is negative.

Sample size	Patients taken from a Phase II clinical trial of neoadjuvant immunotherapy (OpACIN-neo and PRADO extension cohort (NCT02977052)). All available biospecimens were used. Sample sizes are indicated in the figure legends and described in Methods. 16S sequencing was performed on n=103 samples, metagenomic sequencing was performed on n=38 samples (Australian patients enrolled on OpACIN-neo trial)
Data exclusions	No data were excluded. All patients will available biospecimens were included.
Replication	The clinical findings cannot be replicated as all samples were obtained from a clinical trial. Analysis was additionally conducted on publicly available datasets.
Randomization	The cohort utilized is a prospective trial population selected according to enrolment on the OpACIN-neo and PRADO clinical trials (NCT02977052). For the OpACIN-neo trial patients were randomly assigned in a 1:1:1 ratio to receive neoadjuvant treatment with one of three dosing schedules with ipilimumab and nivolumab. PRADO utilized a single arm trial design therefore randomization is not relevant.
Blinding	For the OpACIN-neo trial pathologists were masked to the treatment allocation and all other data in scoring. PRADO trial no blinding was required as no randomisation.

## Reporting for specific materials, systems and methods

We require information from authors about some types of materials, experimental systems and methods used in many studies. Here, indicate whether each material, system or method listed is relevant to your study. If you are not sure if a list item applies to your research, read the appropriate section before selecting a response.

### Materials & experimental systems

- |                                     |   |
|-------------------------------------|---|
| n/a                                 | Involved in the study   |
| <input checked="" type="checkbox"/> | <input type="checkbox"/> Antibodies                             |
| <input checked="" type="checkbox"/> | <input type="checkbox"/> Eukaryotic cell lines                  |
| <input checked="" type="checkbox"/> | <input type="checkbox"/> Palaeontology and archaeology          |
| <input checked="" type="checkbox"/> | <input type="checkbox"/> Animals and other organisms            |
| <input type="checkbox"/>            | <input checked="" type="checkbox"/> Human research participants |
| <input type="checkbox"/>            | <input checked="" type="checkbox"/> Clinical data               |
| <input checked="" type="checkbox"/> | <input type="checkbox"/> Dual use research of concern           |

### Methods

- |                                     |   |
|-------------------------------------|---|
| n/a                                 | Involved in the study                           |
| <input checked="" type="checkbox"/> | <input type="checkbox"/> ChIP-seq               |
| <input checked="" type="checkbox"/> | <input type="checkbox"/> Flow cytometry         |
| <input checked="" type="checkbox"/> | <input type="checkbox"/> MRI-based neuroimaging |

## Human research participants

Policy information about [studies involving human research participants](#)

### Population characteristics

All patients had RECIST-measurable stage III cutaneous melanoma, with local lymph node involvement only, no in-transit disease, no previous immunotherapy, normal LDH and ECOG 0-1. All patients were treated with nivolumab (anti-PD1) combined with ipilimumab (anti-CTLA4). All patients were 18 years or older (range 19-75), 67% were male, 33% were female. Stool samples were available from 71 patients from Australia and 32 patients from the Netherlands

### Recruitment

All patients with clinically detected stage III nodal melanoma who were treated at one of the participating centres and were deemed eligible for the study were invited to participate. Patients were recruited by either surgical oncologist or medical oncologist from the Melanoma Institute Australia or the Netherlands Cancer Institute. Patients with available stool samples were included in the microbiome analyses.

### Ethics oversight

Medical ethics review committee of the Netherlands Cancer Institute and ethical committees at Melanoma Institute Australia approved the trial. The trial was conducted in accordance with the protocol and Good Clinical Practice guidelines as defined

by the International Conference on Harmonization and the Declaration of Helsinki. All participating patients provided written informed consent before enrolment.

Note that full information on the approval of the study protocol must also be provided in the manuscript.

## Clinical data

Policy information about [clinical studies](#)

All manuscripts should comply with the ICMJE [guidelines for publication of clinical research](#) and a completed [CONSORT checklist](#) must be included with all submissions.

Clinical trial registration NCT02977052

Study protocol Protocol is cited within the manuscript and previously published in Lancet Oncology 2019 and Nature Medicine 2021 & Nature Medicine 2022.

Data collection Patients were recruited by 24 November 2016 to 28 June 2018, in Netherlands and Australia

Outcomes The primary endpoints were the proportion of patients with grade 3–4 immune-related toxicity within the first 12 weeks and the proportion of patients achieving a radiological objective response and pathological response at 6 weeks. Analyses were done in all patients who received at least one dose of study drug. Secondary endpoint was relapse free survival. Exploratory endpoints were correlation of the primary and secondary endpoints with stool analysis.